Purification and characterisation of post-consumer plastic pyrolysis oil fractionated by vacuum distillation

Waheed Zeb[1], Martijn Roosen[1], Pieter Knockaert[1], Sven Janssens[2], Daniël Withoeck[3], Marvin Kusenberg[3], Joël Hogie[1], Pieter Billen[2], Serge Tavernier[2], Kevin M. Van Geem[3], Steven De Meester[1]*

[1] Laboratory for Circular Process Engineering (LCPE), Department of Green Chemistry and Technology, Faculty of Bioscience Engineering, Ghent University, B-8500 Kortrijk, Belgium;

[2] Research Group Intelligence in Processes, Advanced Catalysts and Solvents (iPRACS), Faculty of Applied Engineering, University of Antwerp, B-2020 Antwerp, Belgium;

[3] Laboratory for Chemical Technology (LCT), Department of Materials, Textiles and Chemical Engineering, Faculty of Engineering & Architecture, Ghent University, B-9052 Zwijnaarde, Belgium;

*Corresponding author: Steven.DeMeester@UGent.be

List of Abbreviations

AET	Atmospheric equivalent temperature
ASTM	American Society for Testing and Materials
C number	Carbon distribution
CHNSO	Carbon, hydrogen, nitrogen, sulfur, and oxygen
COT	Steam cracker oil temperature
EVA	Ethylene vinyl acetate
EVOH	Ethylene vinyl alcohol
FT-IR	Fourier transform infrared spectroscopy
GC-MS	Gas chromatography-mass spectrometry
IC	Ion chromatography
ICP-OES	Inductively coupled plasma with optical emission spectrometry
IL	Industrial limit
LAOs	Linear alpha olefins
LOD	Limit of detection
LOQ	Limit of quantification
MPO	Mixed polyolefins
MW	Molecular weight distribution
PA	Polyamide
PE	Polyethylene
PET	Polyethylene terephthalate
PIONA	Paraffins, iso-paraffins, olefins, naphthenes, and aromatics
Post-consumer plastic	Waste plastic no longer required for the intended purpose
PP	Polypropylene
ppm	Parts per million
PS	Polystyrene
PVC	Polyvinylchloride
PVDC	Polyvinylidene chloride
TAN	Total acid number
TGA	Thermogravimetric analysis
ΔT	Temperature gradient

Highlights

- Purification of waste plastic pyrolysis oils via vacuum distillation is possible.
- Light and middle fractions contain (<2.5%) metals .
- High total acid numbers, similar densities, and viscosities compared to fossil oils.
- Chlorine, nitrogen, and oxygen are still present in fractions after distillation.
- Distilled fractions are potential feedstock for steam crackers and precursors for chemicals.

Abstract

Valorisation of post-consumer plastic pyrolysis oil in steam crackers and their application as precursors to chemicals is currently hindered by the complexity of these oils in terms of their boiling range, the risk of fouling by unsaturated compounds, and the presence of contaminations (heteroatoms, metals, and halogens). To gain insights into which of these challenges is actually a potential showstopper, we have studied the vacuum distillation of pyrolysis oil derived from two sorted post-consumer waste plastics, i.e. polypropylene (PP) rigids and mixed polyolefins (MPO) rigids, in a batch fractionating column. The crude pyrolysis oil samples were distilled in three fractions i.e., the light fraction (final boiling point <175 °C), middle fraction (175–360 °C), and heavy fraction (initial boiling point >360 °C). Subsequently, comprehensive characterisation, such as physicochemical properties, the level of contaminations, and chemical composition, was performed. The suitability of the light and middle fractions for steam cracking and precursors to chemical feedstock was assessed. It was found that the density and viscosity values of light and middle fractions from the two pyrolysis oil samples were comparable to fossil naphtha and diesel, whereas total acid number (TAN) values were notably higher compared to petroleum-based oil fractions (>0.5 mgKOH/g). Analyses via GC-MS and ATR-FTIR revealed predominant concentrations of olefins. ICP-OES

analysis showed that distillation removes more than 97.5% of metals in all fractions. The chlorine content (>3 ppm), nitrogen (≥0.1%), and oxygen (≥0.1%) exceed thresholds. Hence, this study shows that vacuum distillation effectively improved most, but not all, of the properties of the distilled fractions and can thus be an essential downstream process step for the application of post-consumer plastic pyrolysis oils as feedstock in steam crackers and precursors to chemicals.

Graphical abstract

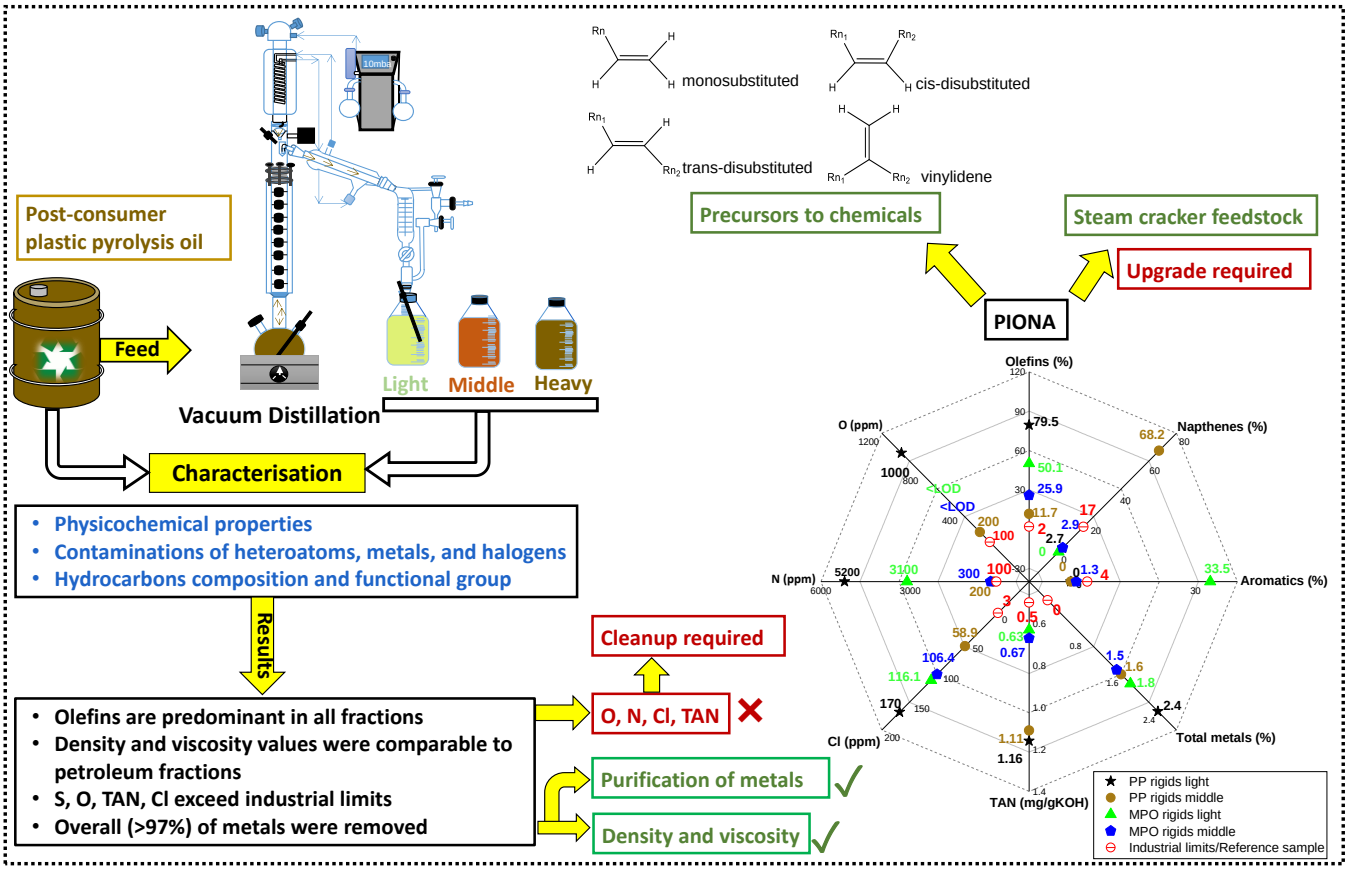

Keywords: Plastic waste, Pyrolysis; Distillation; Characterisation; Contamination; Recycling

1. Introduction

Global plastic production has increased enormously due to population growth, industrialisation, and increasing welfare (Al-Salem et al., 2010). In 2021, 390.7 million tons of plastics per year were produced worldwide. (Plastic Europe, 2022). Proper management of plastic waste remains an enormous global challenge. The largest share of post-consumer plastic waste is packaging material, which accounts for approximately 42% of global plastic production (Geyer et al., 2017). Packaging plastic waste mostly comprises polyethylene (PE), polypropylene (PP), polyethylene terephthalate (PET), polystyrene (PS), MPO (which is a mixture of PP and PE rigids, for example, created as float fraction in plants processing mixed plastics) as discussed by Kleinhans et al. (2021) and combinations of those with some lower concentrations of other polymers added in multilayer structures such as polyamide (PA) and ethylene vinyl alcohol (EVOH) (Chen et al., 2021). Post-consumer plastic includes both flexible films, for example, plastic bags and pallet wrap and rigids plastic: any plastic having a relatively inflexible form and can maintain its shape, whether empty or full, under normal usage such as, bottles and trays (Rigids plastic, 2023).

Plastic recycling mainly depends on the composition of post-consumer plastic waste. For instance, mechanical recycling is an effective technique widely applied and proven at an industrial scale because of its simplicity, economic balance, and potential environmental benefit (Ragaert et al., 2017). However, mechanical recycling is mostly efficient for homogenous polymers and has disadvantages, such as (thermal) degradation and loss of certain properties during processing due to impurities including wood paper, inks and additives. On the top of this post-consumer waste also contains other polymers. This makes high-end

recycling routes challenging to achieve via mechanical recycling and often limits the use of recyclates to low-end applications (Roosen et al., 2020;Horodytska et al., 2018).

Chemical recycling of post-consumer plastic waste by thermal pyrolysis is a promising alternative to mechanical recycling as it offers advantages, such as the possible treatment of a broad range of plastics and mixed polymers (Ragaert et al., 2017). Thermal pyrolysis is a process in which long-chain polymer molecules break down into smaller ones by thermal degradation in an oxygen-free environment (Czajczyńska et al., 2017). Typically, pyrolysis produces light gases having carbon numbers ranging from C_1 to C_4, liquid products (longer hydrocarbon fractions, including waxes), and solid char particles. The liquid product (pyrolysis oil) is a mixture of hydrocarbons having a wide carbon distribution typically ranging from C_5 to over C_{50} strongly depending on the pyrolysed polymers and the chosen pyrolysis conditions. For instance, PP pyrolysis leads to higher carbon numbers due to a high degree of branching in the obtained hydrocarbon matrix. On the other hand, PS decomposes predominantly to styrene mono and oligomers and hence to lower carbon number products (Al-Salem et al., 2010;Kusenberg et al., 2022e). When the feedstock contains impurities of halogen, metal, and heteroatomic compounds of oxygen, nitrogen, and sulphur, these also end up in these fractions (Dao Thi et al., 2021).

Pyrolysis oils have several applications for example, Mangesh et al. (2020) studied the direct application of plastic pyrolysis oil and fossil diesel blend in a diesel engine. Park et al. (2020) focused on the recovery of chemicals (xylenes, toluene, benzene, ethylbenzene, and styrene) from pyrolysis oil derived from polystyrene. Furthermore, developments are in progress for the integration of plastic pyrolysis oil in conventional refineries, such as at the ReOil pilot plant by OMV Austria (ReOil, 2021) and Plastic Energy Spain (Plastic Energy) in which plastic pyrolysis oil production is piloted. Pyrolysis by-products can be valorised in several

applications; for example, light gases can be used for energy generation, while char is useful as a potential adsorbent (Sharuddin et al., 2016;Jamradloedluk and Lertsatitthanakorn, 2014). Thermal decomposition options such as pyrolysis look attractive because incorporating the pyrolysis oils might not require major alterations in existing refinery and petrochemical infrastructure. Such an evolution in chemical recycling would allow closing of the material loop: from waste plastics to high-quality (virgin grade) new plastics.

Currently, there are several challenges in the valorisation of post-consumer plastic pyrolysis oil on commercial scale towards high-end refining. These include the wide carbon distribution, complexity of hydrocarbons (unsaturation), and the risk of fouling and clogging due to the presence of contaminations in pyrolysis oil which are considered problematic for further downstream processes such as, fuel applications, steam cracking and isolation of chemicals (Lopez et al., 2017). For example, PET impurities tend to produce terephthalic acid and benzoic acid, which cause blockages in condensing sections, whereas halogens and heteroatoms cause corrosion and catalyst poisoning in reactors (Meys et al., 2020). Furthermore, metals lead to coke formation and downstream catalyst poisoning in steam cracking (Symoens et al., 2018). Therefore, the need for refining pyrolysis oils by fractional distillation is considered a main step towards fuel applications, steam cracking, and conversion to chemicals, whether or not combined with other purification techniques such as extraction and hydrotreatment.

Distillation of pyrolysis oil derived from plastic has been studied recently by several researchers for fuel applications (Lee et al., 2021;Thahir et al., 2019;Jahirul et al., 2022). However, the suitability of distilled products for steam cracking and precursors to chemicals is still further to be explored. In addition, previous studies have focused on simple atmospheric distillations that resulted in cracking reactions at higher temperatures and lead to poor separation (overlapping of heavy components in the lighter cuts) which causes overheating of

the convection section of steam crackers (Kusenberg et al., 2022c;Faussone, 2018;Faussone and Cecchi, 2022). Hence, more insight in the characterisation and purification aspects of vacuum distillation is crucial for designing downstream processes and obtaining more end-market opportunities for pyrolysis products.

The main objective of this work is to investigate fractions obtained from the vacuum distillation of two plastic pyrolysis oils distilled each into three fractions i.e., a light fraction (final boiling point ≤175 °C, C_5-C_{10}; naphtha cut), a middle fraction (175-360 °C, C_{10}-C_{21}; diesel cut) and a heavy fraction (initial boiling point ≥360 °C, C_{20+}; vacuum gas oil). The produced fractions have thus similar boiling point ranges as petroleum-derived fuel fractions. The distilled fractions were comprehensively characterised by (1) comparing the yield of the fractions obtained via fractional vacuum distillation of two pyrolysis oils. (2) Investigating the physicochemical properties (i.e., viscosity, density, and total acid number) by comparing them with fossil-based naphtha and diesel. (3) Examining the level of contaminants (i.e., metals, halogens, and heteroatoms). (4) Analysing hydrocarbon compositions and chemical functional groups. (5) Assessing the suitability of distilled fractions as feedstock in steam crackers and precursors to chemicals.

2. Materials and methods

2.1 Pyrolysis oils and reference petroleum fractions

Prior to pyrolysis, two post-consumer plastic waste fractions (PP rigids and MPO rigids) were collected at curb-side in Belgium, representing typical household plastic waste. The chosen fractions were pre-treated by Ecoo (Belgium) in a sorting facility such as, washing, float sinking and regranulation. Basically, some would call this mechanically recycled already, but the number of applications is limited, given limitations in colours, odours, compatibility, and resulting mechanical property loss. Hence, this study chose these fractions as feedstock to

increase their potential for substituting plastics in broader applications. The chemical composition of PP rigids plastic was PP-87.5%, PE-12.5% and others (PET, PA, EVA, EVOH, PVC) <0.1%, whereas MPO rigids consisted out of PP-46.2%, PE-52.9% and others (PS, PET, PA, EVA, EVOH, PVC) 0.9% as reported by (Kusenberg et al., 2022d;Roosen et al., 2020). Afterward, these samples were fed to a pilot-scale pyrolysis unit. The feed was processed at 450 °C and atmospheric pressure. The residence time of the sample in the reactor was 45 min. (Kusenberg et al., 2022d;Zayoud et al., 2022). The pyrolysis setup is shown as Fig. S1 in the SI. The additive-free petroleum-based reference crude oil, naphtha, and diesel fractions were obtained from a petrochemical company in Belgium. The obtained naphtha and diesel were products of a crude atmospheric distillation tower.

2.2 Vacuum fractional distillation of pyrolysis oil

2.2.1 Distillation setup

The present study was carried out in a batch distillation setup, as shown in Fig. 1. The setup comprises a heating mantle with adjustable power and a temperature range up to 450 °C, equipped with a round bottom boiling flask having a capacity of 5 L (1,2). The flask has two necks; one for the feed and relief valve and the other for the temperature sensor (3,4). The distillation column has a diameter of 50 mm and height of 1350 mm and is filled with structured packing Montz-Pak Type B1-350 (Germany). The packing has a height of 1200 mm and a diameter of 47 mm, equivalent to eight theoretical plates (5). Furthermore, the boiling flask is equipped with a heater top to prevent heat loss. The column is also equipped with a magnetic reflux splitter and vapour temperature prob (6,7). The overhead condenser can operate between -20 and 130 °C and can thus be used to condense lighter components and heat the heavy fractions to avoid solidification using a chiller (8). A fraction collector with a volume of 500 mL is used to collect distilled fractions (9) . Two dry ice traps were used to catch very light hydrocarbons, protecting the vacuum pump (LVS -Welch, Germany) and pressure sensor from

damage (12,14,15). The pot temperature T-1 (4), vapour temperature T-2 (6), receiver temperature T-3 (10), vacuum sensor reading P-1 (16), and reflux ratio were recorded in the LABVIEW program (17).

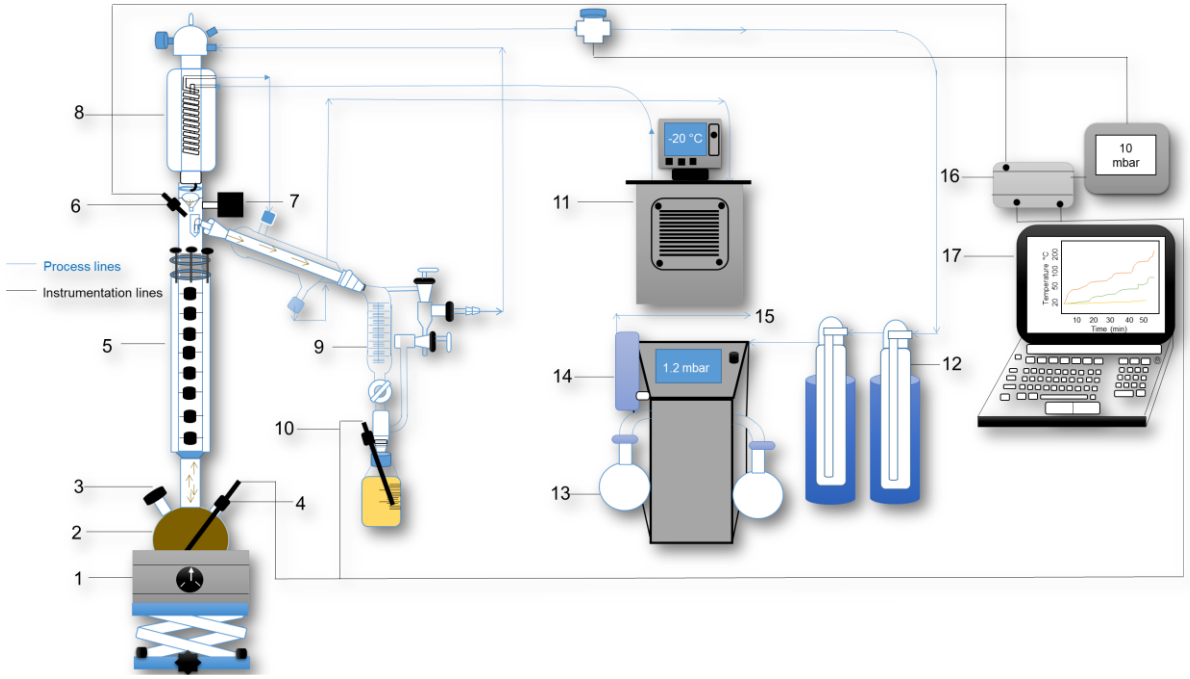

Fig. 1: Batch distillation setup: Heating mantle, (2) Boiling flask; 5 L, (3) Feed and relief valve; V-1 (4) Temperature sensor of the boiling flask; T-1 (5) Double jacketed and insulated fractionating column; C-1, (6) Temperature sensor of vapour; T-2, (7) Magnetic reflux splitter, (8) Condenser, (9) Fraction collector, (10) Temperature sensor of receiving flask; T-3, (11) Chiller, (12) Dry ice vacuum traps, (13) Atmospheric vapour traps, (14) Vacuum pump, (15) Vacuum pump exhaust, (16) Signal transmitter, (17) Recording device.

2.2.2 Distillation procedure

Firstly, test runs were conducted using ethanol to clean and dry the setup and examine the correct working of the temperature, pressure sensor, and reflux valve. Typically, 5 L of pyrolysis oil was heated in a water bath to allow feeding in the liquid state. After hot feeding, boiling stones were added for homogeneous operations during the distillation. At the beginning of the vacuum distillation, the condenser temperature was set to -20 °C to condense light hydrocarbons in the pyrolysis oil (typically<C_7) as defined in the ASTM D2892 (2019) procedure to avoid their flow toward the pump and sensor. At the start of the distillation, the

power was set to 50% of 1,2 kW at total reflux. In one hour, equilibrium was established, and the column was switched to refluxing at 1:1 ratio. After collecting the light fraction, the condenser temperature was increased to 25 °C and electrical power to 80%. Next, the condenser temperature was adjusted to 80 °C and electrical power to 100%, when the distillation temperature reached 300 °C atmospheric equivalent temperature (AET) as shown in Table. 1. Increasing the condenser temperature prevents the higher boiling fraction from solidifying on the surface of the condenser. When the vapour temperature reached the desired boiling point range, the product from the fraction collector was transferred to the receiving flask to switch to the next fraction. With increasing distillation temperature, the gradient between boiling and vapour temperature varies from ΔT = 70 °C to 90 °C also discussed by Lee et al. (2021). All distillation experiments were performed at reduced pressure (10 ± 2 mbar) as a preventive measure to avoid recovery loss due to cracking reactions at high temperatures and to obtain a full diesel range cut

Table 1: Parameters for vacuum distillation

Fraction	Electrical power (1200 W)	Operating pressure (mbar)	Reflux ratio	Condenser temperature T-4 (°C)	Bottom (boiling) temperature T-1 (°C)	Top (vapour) temperature T-2 (°C)	Atmospheric equivalent vapour temperature AET (°C)
Light	50%	10±2	1:1	-20	50-123.7	16-52.2	<175
Middle							
AET <300°C	80%	10±2	1:1	25	124-240	52.2-153	175-300
AET>300°C	100%	10±2	1:1	80	240-293.4	153-202.6	300-360

2.3 Analytical methods

2.3.1 Physicochemical properties

The density of liquid and solid samples was measured with a Quantachrome ultrapyc 1200e gas pycnometer using a small sample cell (7 cm^3). Helium 5.0 (Air Liquide, Belgium) was used

first to rinse the sample cell and later to bring it under pressure (approx. 19 psi). at 15 °C. The temperature was measured and reported for each experiment. Measurements were automatically repeated until a maximal deviation of 0.05% was achieved. The instrument reported the average of the last 5 measurements. The density of the liquid samples was also analysed by Mettler Toledo Densito U-tube densitometer for verification. Viscosity measurements were performed using an Anton-Paar SVM-3001 viscometer according to ASTM D7042. Total acid number (TAN) was determined according to ASTM D664 using a Mettler Toledo T50 auto-titrator.

Thermo gravimetric analysis of the char particles (TGA) was performed with a NETZSCH TG 209 F3 Tarsus® analyser. Around 20 mg of the sample was heated from 25 to 700 °C at a heating rate of 10 °C/min and a nitrogen flow of 20 ml/min (Rannaveski et al., 2016).

2.3.2 Contaminants analysis (metals, halogens and heteroatoms)

Metal analysis was performed using ICP–OES equipped with Qtegra Software (Thermo Scientific iCAP 7000 Plus Series ICP–OES, Thermo Fisher Scientific Brand, USA) and with a CETAC AXP 560 autosampler (Teledyne Technology, USA). Firstly, calibration standards (ranging from 0.001 ppmw up to 20 ppmw) were prepared by Certipur multi-element standard solutions (100 mgL^{-1} in 10% HNO_3), comprising Cd, Cu, Co, Zn, Fe, Mn, Pb, Li, Mg, Sr, Sb, Ti, Ca, Cr, As, Se, Al, Na, Be, Ni, Tl, Si, and V. The samples were digested with an Anton Paar (Graz, Austria) Multiwave 5000 microwave oven equipped with a 20SVT-rotor and PTFE-TFM digestion vessels. 0.50 ± 0.05 g of each sample was weighed in a digestion vessel prior to digestion and ICP–OES analyses. 10.0 mL of concentrated HNO_3 (7%, Sigma Aldrich) and 3.0 mL of double-distilled water were added to the weighted sample. The vessels were transferred to the microwave oven and subjected to the following heating program: 20 min ramping time up to a temperature of 200 °C and 15 min heating time. After digestion, the samples were diluted to a volume of 50 mL with double-distilled water. Blanks were prepared

using the same procedure without the addition of a sample. Afterwards, the samples were filtered using a syringe filter (0.45 μm syringe filter, PP filter media, CHROMAFIL). The limit of detection (LOD) of the ICP–OES analysis was quantified by multiplying the standard deviation of the blank by 3. The limit of quantification (LOQ) was quantified by multiplying the standard deviation of the blank by 10. The values for the LOD and LOQ are given in Table S2 in the SI.

Halogen analysis was performed using ion chromatography (IC). Prior to analysis, the samples (0.1000 ± 0.0100 g) were digested in a microwave equipped with an oxygen-combustion set (Multiwave 5000, Anton Paar, Graz, Austria) and an 8NXQ80-rotor and PTFE-TFM digestion vessels. After that, the digested samples were diluted to a total volume of 50 mL. Next, the samples were analysed with an ion-chromatograph (930 Compact IC Flex, Metrohm, Herisau, Switzerland), equipped with a Metrosep A Supp 7-250/4.0 column and conductivity detector. Linear calibration curves using 5 standard solutions in the range of 0 and 50 ppmw of the analytes of interest were used to quantify the halogen concentration. The limit of detection (LOD) and the limit of quantification (LOQ) were quantified by multiplying the standard deviation of the blank by 3 and 10, respectively. The LOD and LOQ values are given in Table. S2 in the SI. CHNS/O analyses were performed using a Flash EA2000 elemental analyser (Interscience, Belgium) equipped with a thermal conductivity detector (TCD). The measurement of CHNS was performed in combustion mode according to ASTM D5291 standard method. Oxygen analysis was performed in pyrolysis mode in a separate reactor according to ASTM D5622.

2.3.3 Hydrocarbon composition and chemical functional groups (GC-MS & FT-IR)

Gas chromatography-mass spectrometry (GC–MS) was applied to identify hydrocarbons in the pyrolysis oil and derived fractions. Prior to analysis, samples were dissolved in diethyl ether (99%, Sigma-Aldrich, Belgium) with a dilution factor of 1:25. The used solvent was spiked

with 50 ppm of the internal standard 3-chlorothiophene (98%, Sigma-Aldrich, Belgium). Subsequently, the solution was transferred into a 1.5 mL microvial. Afterward, 1 µL of the spiked solution was injected in splitless mode via a Supelco split/splitless type wool packed liner with a single taper design into an Agilent 6890 GC coupled to a Hewlett Packard mass-selective detector 5973 equipped with cross-linked (5%-Phenyl)-methylpolysiloxane (HP-5 ms, Agilent) column (30 mm × 0.25 mm, 0.25 µm). The initial temperature of the injection port was set at 300 °C. Helium was used as a carrier gas with a linear flow rate of 1 mL/min. The oven program was set as follows: 30 °C for 3 min, an increase to 350 °C at 5 °C/min, which was maintained for 10 min. The components were identified based on their mass spectra (NIST mass spectral library).

Based on the tentatively identified components, a Selective Ion Monitoring (SIM) method was developed for quantitative analysis using the same GC–MS parameters and program. The weight fraction of each compound is calculated based on the known amount of internal standard explained in detail elsewhere (Djokic et al., 2012;Van Geem et al., 2010;Diaz-Silvarrey et al., 2018;Dijkmans et al., 2015). Data analysis was performed via the Agilent MSD Chemstation software. Detailed PIONA (Paraffins, Iso-paraffins, Olefins, Naphthenes and Aromatics) were grouped based on quantitative analysis.

Chemical functional groups were analysed on Bruker Alpha ATR-FTIR spectrometer equipped with a diamond crystal. The spectral range was between 4000 cm^{-1} and 600 $cm^{-1,}$ with a resolution of 4 cm^{-1}. All spectra result from an average of 24 scans.

2.3.4 Steam cracking using COILSIM1D simulations

The performance of PP rigids and MPO rigids distilled fractions in a steam cracker has been studied using the commercial steam cracking simulation package COILSIM1D (Symoens et al., 2018;Plehiers et al., 2019). Detailed PIONA analysis obtained from GC-MS (Table. S4 in the SI) was used as input to the process simulator. The reactor geometry and simulation process conditions were obtained from previous experimental studies using a bench-scale steam cracking unit (Kusenberg et al., 2022a). Steam cracker yields of distilled fraction were compared with fossil naphtha at two temperature profiles (COT: 820 °C & 850 °C) to mimic with industrial operation.

3. Results and discussions

3.1 Recovery of distilled fractions

Fig. 2 represents the recovery (vol%) of fractions by vacuum fractional distillation of the two pyrolysis oil samples. The recovery of light fraction from PP rigids was 30.0% as compared to 22.4% from MPO rigids. This is because pyrolysis of PP-based oils typically comprises lower molecular weight and branched hydrocarbons (Kusenberg et al., 2022e). Similar recoveries are observed between the two samples in the middle fraction, 38.0% and 35.0% for PP rigids and MPO rigids, respectively. The heavy fraction was 29.6% for PP rigids, and 40.4% for MPO rigids. A minor volume loss could be noted due to column holdup after distillation runs and evacuation of vapours by the pump during vacuum conditions. By the end of the distillation run, solid char particles were also obtained at the bottom of the boiling flask. The char produced in the boiling flask was 0.23% for PP rigids and 0.56% for MPO rigids. MPO rigids resulted in more char, possibly due to high impurities in the original waste sample. Due to prolonged high temperatures in the boiling flask, char particles also tend to form an agglomeration of polymerised products (gum formation) as shown in Fig S2 in the SI (Seo et al., 2003). TGA

was applied to characterise char particles. 87.3% of the total sample were volatile matters, whereas the fixed solids in the TG pan were 12.7%, as shown in Fig.S4 in the SI. The overall recovery was more than 97.8% in both cases.

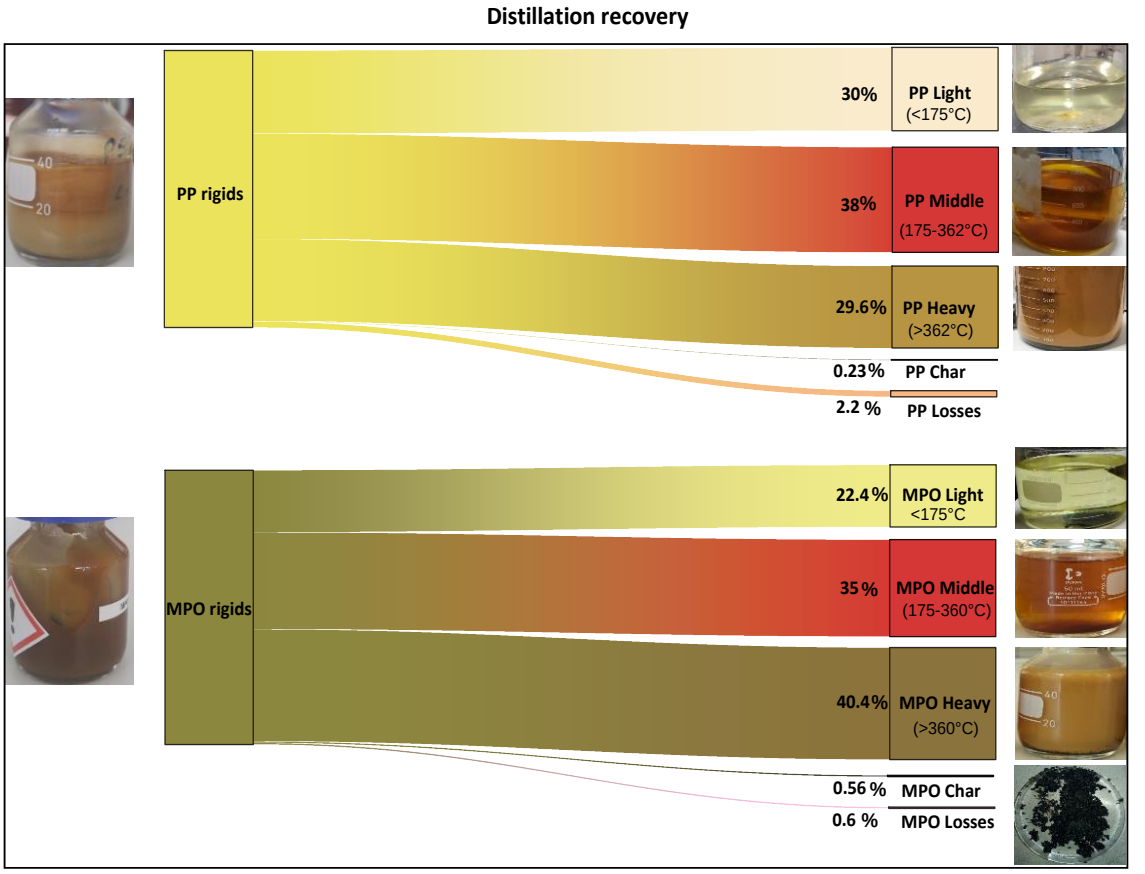

Fig. 2: Vacuum distillation recovery (vol%) for PP rigids and MPO rigids pyrolysis oils

Fig.2 also shows that both PP rigids and MPO rigids pyrolysis oils are brownish and waxy at room temperature. This is because pyrolysis oil from polyolefins obtained at atmospheric pressure and 450 °C produces waxy products (Kusenberg et al., 2022d). The light fractions have a boiling temperature below <175 °C and exhibit a clean and slightly yellowish appearance compared to typically colourless petroleum naphtha (Speight, 2019). The middle fractions, having a boiling point range of 175–360 °C, resulted in a slightly viscous brownish liquid comparable to petroleum diesel. The heavy fractions collected in the boiling flask after

distillation with a boiling point range above 360 °C have a relatively dark brown colour and are hard waxy at room temperature.

3.2 Physicochemical properties

Physicochemical properties such as density, viscosity, and total acid number (TAN) of the two pyrolysis oils and obtained distilled fractions were analysed and compared with corresponding additive-free petroleum crude oil, naphtha and diesel as summarised in Table.2 and Fig.3.

The density of PP light was measured as 0.76 g/cm^{3,} comparable with the reference fossil naphtha, while MPO light was slightly higher at 0.79 g/cm^3. This could be attributed to high amounts of aromatics in the MPO light, as shown in Fig.6. Aromatics have high densities compared to other hydrocarbons due to ring structure, multiple bonds, and planar geometry causing an increase in the density (Karonis et al., 1998). The densities of the middle fractions from the two pyrolysis oils (PP rigids: 0.80 g/cm^3 and MPO rigids: 0.81 g/cm^3) were slightly lower than the reference diesel (0.83 g/cm^3) and the European standard EN 590:2009 (0.82-0.84 g/cm^3) (European Committee, 2013;Sher, 1998). Like the middle fractions, the densities of crude pyrolysis oils from the two waste samples were also lower than fossil crude oil. The lower densities of the heavy fractions and crude pyrolysis oil could be attributed to lighter unsaturated hydrocarbons compared to fossil diesel and crude petroleum oil, mainly containing paraffins (Gala et al., 2020).

The kinematic viscosities of the distilled fractions and fossil naphtha and diesel were analysed at 40 °C. The viscosities of the light fractions from PP rigid were 0.8 cSt, and MPO rigids were 0.6 cSt, slightly higher than that of fossil naphtha. A possible reason is the high concentration of (branched) olefins and iso-paraffines in PP light as compared to MPO light, as shown in Fig.6. Branching can lead to higher viscosities due to increased molecular volume, friction between the molecules, and shape complexity, leading to higher intermolecular forces and

therefore, higher viscosity (Yan et al., 1999). The viscosity of the middle fraction from PP rigids was 2.9 cSt, which is relatively high compared to MPO rigids at 2.3 cSt and fossil diesel at 2.4 cSt. A possible reason could be the presence of higher naphthenes. Naphthenes with large ring sizes or fused ring systems can have a higher molecular volume and more complex shape than smaller naphthenes, leading to higher intermolecular forces and, thus, higher viscosity (Knothe and Steidley, 2005). The viscosities of middle fractions from the two types of materials are in good agreement with the limits for diesel or diesel-like fuel according to EN 590:2009 standard (2.0-4.5 cSt at 40 °C), developed by the European Committee for Standardisation (Murphy et al., 2012).

Table 2: Physico-chemical properties of two pyrolysis oil fractions and reference samples

Properties	PP rigids light	MPO rigids light	Fossil based naphtha	PP rigids middle	MPO rigids middle	Fossil based diesel	PP rigids heavy	MPO rigids heavy	PP rigids pyrolysis oil	MPO rigids pyrolysis oil	Crude oil
Density g/cm^3 at 15.5 ± 0.3 °C	0.76	0.79	0.76	0.80	0.81	0.83	0.85	0.86	0.82	0.84	0.87
Kinematic viscosity cSt at 40 °C	0.8	0.6	0.6	2.9	2.3	2.4	[a]	[a]	[a]	[a]	3.3
Boiling range °C	69-175	69-175	75-170	175-362	175-360	155-370	362+	360.5+	[b]67-473	[b]65-403	[b]66-500
Carbon range C number	≤C_{10}	≤C_{10}	C_4-C_9	C_{10}-C_{21}	C_{10}-C_{21}	C_9-C_{22}	≥C_{21}	≥C_{21}	[b]C_6-C_{32}	[b]C_6-C_{25}	[b]C_5-C_{36}

[a] Wax at the measurement temperature.
[b] The final boiling point and carbon number could be higher for pyrolysis oils and crude oil due to the maximum temperature limitation of 350 °C for the GC column.

TAN is a crucial property of pyrolysis oil that depicts the corrosion potential and stability of the oil during storage and applications (Alvisi and Lins, 2011). Oils with a TAN value greater than 0.5 mgKOH/g are highly acidic (Zhang et al., 2006). Fig. 3 shows that TAN values for all the pyrolysis-derived fractions were higher than fossil-based naphtha and diesel exceeded the threshold value. A possible reason could be the presence of oxygenates and chlorides in the fractions, confirmed by GC and IC analysis. Overall, TAN values of PP fractions were notably higher as compared to MPO rigids fractions. A likely cause for higher TAN might be the reactivity of olefins in PP fractions and oxidation of reactive double bonds, possibly forming oxygenated acids (Majano et al., 2011;George Wypych, 2015).

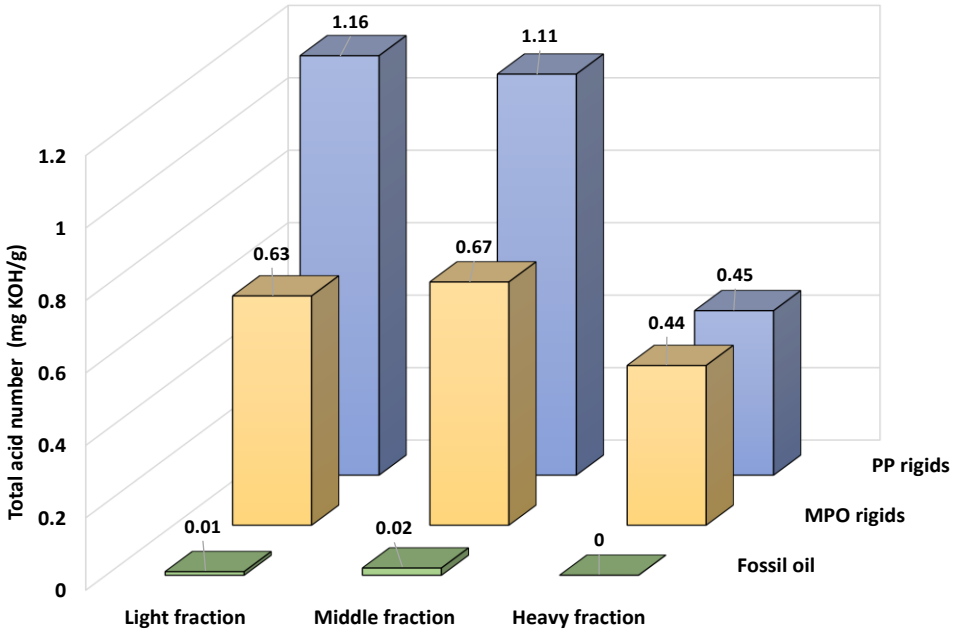

Fig.3: Comparison of Total Acid Number (TAN) of the two-pyrolysis oil-derived fractions, naphtha and diesel (light and middle fraction of fossil-oil corresponds to naphtha and diesel, respectively).

3.3 Overview of contaminants (metals, halogens, and N, S, O)

Post-consumer pyrolysis oil typically contains metals, halogens, and heteroatoms derived from additives and laminates in the plastic, heterogeneous plastic, and contaminations during production, use, and waste management. Based on previous study on contaminations in pyrolysis oil, metals (Al, As, Be, Ca, Cd, Co, Cr, Cu, Fe, Hg, Li, Mg, Mn, Mo, Na, Ni, Pb, Sb, Se, Si, Sr, Ti, Tl, V, Zn), halogens (F, Cl, Br) and heteroatoms (N, S, O) contaminants have been analysed (Kusenberg et al., 2022d).

Fig. 4 depicts a comparative overview of metal contaminations in the two pyrolysis oils, distilled fractions and petroleum-based reference naphtha and diesel. The total analysed metal contents of PP rigids and MPO rigids pyrolysis oil were 703.4 ppm and 440.7 ppm, respectively. After distillation, the total metal contents in PP light, PP middle and PP heavy fractions were reduced to 16.9 ppm, 11.2 ppm and 8.9 ppm, respectively, whereas, in the MPO light, MPO middle and MPO heavy fractions were 7.8 ppm, 6.7 ppm and (<LOD) respectively, confirming a clear improvement in the quality of liquid productswhile the lion share of metal

contaminants remains as solid char in the distillation flasks. Compared to fossil naphtha and diesel, the concentration of metals in both MPO rigids and PP rigids fractions was high. Most metals tend to concentrate and accumulate at the bottom of the boiling flask during distillation, while organometallic compounds may volatilise at distillation temperatures in both light and middle fractions (Ali and Abbas, 2006;Yang et al., 2010) . It can be concluded that distillation effectively removed most metals from distillation products. In the char, the highest concentration of metal was Al (23102 ppm), mainly used as a barrier layer in packaging. Another major metal impurity was Fe (5073 ppm), found in certain inks and abrasions from process equipment such as extruders and reactors. Ca and Si impurities originate from SiO_x coating or fillers (e.g., talc contains Si). A detailed overview of the origin of these contaminations can be found elsewhere (Kusenberg et al., 2022a;Ugduler et al., 2020;Roosen et al., 2020).

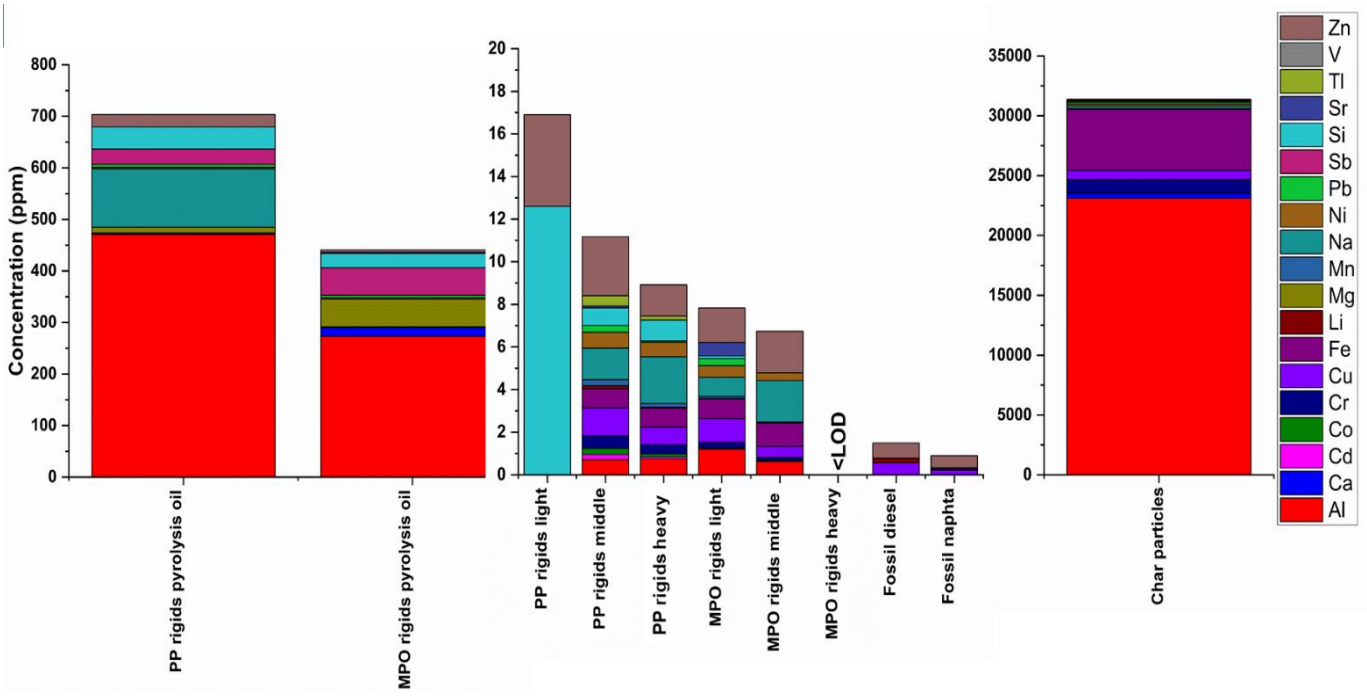

Fig.4: Comparative overview of metals in the two pyrolysis oils, fractions, fossil diesel, and naphtha. Limits of detection (LOD) and quantification (LOQ) can be found in Table.S2 in the SI.

Next to metals, halogens are another vital contamination. Notably, both the pyrolysis oil and fractions contain chlorine in considerable amounts compared to fossil-based samples, as shown

in Fig.5. It was reported that chlorine originates possibly from PVC, PVDC, and NaCl (Kusenberg et al., 2022d;Roosen et al., 2020). Pyrolysis of PVC partly results in the formation of chlorobenzene that ends up in the light fractions. Higher amounts of chlorine in these fractions are highly unfavourable as they can cause corrosion in reactors, process equipment, and fuel engines. The chlorine content for transportation fuel should not exceed 10 ppm (Ragaert et al., 2017). A lower concentration of 3 ppm bromine was detected in the MPO heavy fraction only, which might be attributed to a flame retardant additive contamination adsorbed from a product during the lifetime in this sample, while fluorine was not detected in any samples (Ebnesajjad, 2020).

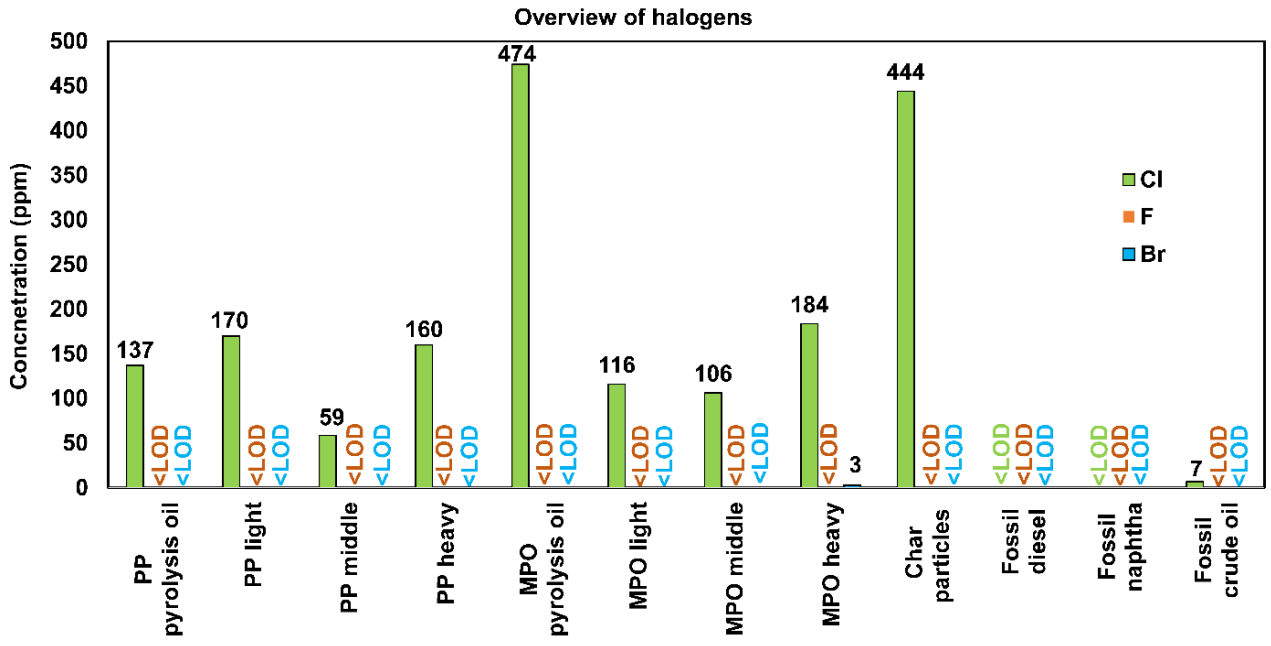

Fig.5: Comparative overview of halogens in the two pyrolysis oils, fractions, diesel, and naphtha.

Furthermore, heteroatoms (i.e. oxygen, nitrogen, and sulphur) content is also crucial when considering the valorisation of pyrolysis oils; for example, oxygen produces acids while sulphur and nitrogen cause poisoning downstream catalyst (Kusenberg et al., 2022b). From Table.3, it can be reported that both pyrolysis oils contain considerable amounts of nitrogen and oxygen. In case of PP rigids, N was present at 0.3% and O at 0.1%. After distillation, N

was found at concentrations of 0.5% and 0.1% and (<LOD), whereas O was found at 0.1%, 0.10% and (<LOD) in the light, middle and heavy fractions, respectively. In case of MPO rigids, N was found at 0.4% and O at 0.1%. After distillation, the analysis showed an N concentration of 0.3% and 0.1% and (<LOD) in the light, middle and heavy fractions, respectively, while O was lower than the detection limit. It can be observed that N and O heteroatom compounds are more pronounced in the lighter fractions. Sulphur was not detected in pyrolysis oils and fractions.

Table 3: Elemental analysis of pyrolysis oil, fractions and fossil-based reference samples

Sample	**Elemental analysis** wt (%)				
	C	**H**	**N**	**O**	**S**
PP rigids light	85.2	14.1	0.5	0.1	<LOD
MPO rigids light	87.3	12.3	0.3	<LOD	<LOD
Petroleum naphtha	84.3	15.7	<LOD	<LOD	<LOD
PP rigids middle	85.6	14.2	0.1	0.1	<LOD
MPO rigids middle	85.7	14.2	0.1	<LOD	<LOD
Petroleum diesel	86.5	13.2	<LOD	<LOD	0.3
PP rigids heavy	85.7	14.3	<LOD	<LOD	<LOD
MPO rigids heavy	85.7	14.3	<LOD	<LOD	<LOD
PP rigids pyrolysis oil	85.4	14.2	0.3	0.1	<LOD
MPO rigids pyrolysis oil	85.8	13.7	0.4	0.1	<LOD
Fossil crude oil	86.6	12.4	0.2	<LOD	0.8

3.4 Hydrocarbon composition

The abundance of compounds and carbon distribution in pyrolysis oil and fractions is represented by GC–MS chromatogram. Fig.6(a) shows hydrocarbon peaks in PP pyrolysis oil and distilled fractions. Hydrocarbons detected in the PP pyrolysis oil and light fraction were mostly olefins, with the highest peak corresponding to C_9 olefins (Ballice and Reimert, 2002). Fractional distillation in the aforementioned distillation conditions allows sharp isolation of $\leq C_{10}$ hydrocarbons corresponding to a boiling range of ≤175 °C (light fraction). Small overlapping peaks were observed at C_{11} due to the co-elution of lower boiling point C_{11} alkenes and C_{10} alkanes (Grams, 2020;Kusenberg et al., 2022d). The middle fraction represents the hydrocarbon range of C_{11}–C_{20} and corresponds to a boiling range of 175–360 °C. The heavy fraction comprises the C_{20+} hydrocarbons, i.e. ≥360 °C boiling range. Especially heavy

hydrocarbons are difficult to measure with many GC techniques due to limited column temperature resistance, relatively low response factor of heteroatomic hydrocarbons, and limited peak capacity. However, some indication of components can be obtained using GC–MS to identify the carbon range of distilled fractions (Kusenberg et al., 2022a).

Fig. 6(b) represents the GC–MS chromatograms for MPO pyrolysis oil and its distilled fractions. The chromatogram follows a typical series of hydrocarbon peaks comprising iso-paraffins intermixed with dienes followed by alkene and alkane peaks in ascending order of carbon range, corresponding to the presence of polyethylene in the original waste plastic sample, while the highest peak at C_9 shows the presence of PP contents in the MPO pyrolysis oil (Chandrasekaran and Sharma, 2019). The MPO crude pyrolysis oil has a broader and more equal distribution of the carbon peaks, which was expected as it was a mix of roughly the same parts PE and PP. Carbon distribution observed in both cases was narrow due to efficient rectification.

Next to the comparative GC–MS to highlight the profile of the distillation cuts, components in the light and middle fractions are grouped based on chemical functionalities, while pyrolysis oil and heavy fractions were not quantified due to the temperature limitation of the GC column. We discuss the composition of light and middle distillates from the two pyrolysis oils compared to fossil-based naphtha and diesel, as shown in Fig.S5 in the SI. Olefins and naphthenes are abundantly present in PP-based fractions, as explained by the fact that PP tends toward the formation of oligomers of isotactic propylene during pyrolysis (Kusch, 2017). The concentration of olefins in the PP light was 72.8%, relatively high compared to 48.6% in the MPO light and only 2% in fossil naphtha. 2,4-dimethyl-1-heptene (C_9) is a predominant compound in the PP light. Aromatics were absent in the PP light compared to 33.5% in MPO light and 34 % in the fossil naphtha. This could be attributed to PS impurities present in the

MPO rigids, as discussed in section 2.1. The concentration of paraffins was 3.2% in PP light lower than 6.1 % in MPO light and 8 % in the fossil naphtha.

In the middle fraction, olefins were present in a lower concentration, being 11.6% in the PP compared to 25.9% in MPO. Paraffins were present at 44.3% in MPO middle compared to 18.8% in PP middle and 41% in fossil diesel. The higher amounts of paraffins and iso-paraffins in the MPO middle can be explained by the presence of PE content and the decomposition chemistry of PE, according to which primary radicals form saturated hydrocarbons (Dogu et al., 2021). It can be noted that the content of naphthenes in the PP middle was unexpectedly high at 67.4%. This might be attributed to the formation of cyclic compounds at high temperatures in the distillation flask. The presence of 6.1% alcohols in the MPO middle could be due to oxygenated impurities in MPO rigids plastic. The high aromatics of 34% in the naphtha and 38.3% in diesel might indicate that the reference samples were aromatic. Similar results of high aromatics in fossil diesel and lower paraffins in pyrolysis-derived light fraction range also discussed by Seo and Shin (2002), who quantified distilled plastic pyrolysis oils. However, fewer aromatic functionalities from ATR-FTIR in this case could be due to co-elution of peaks resulting in poor separation. A more powerful technique such as GC×GC would be useful for detailed analysis.

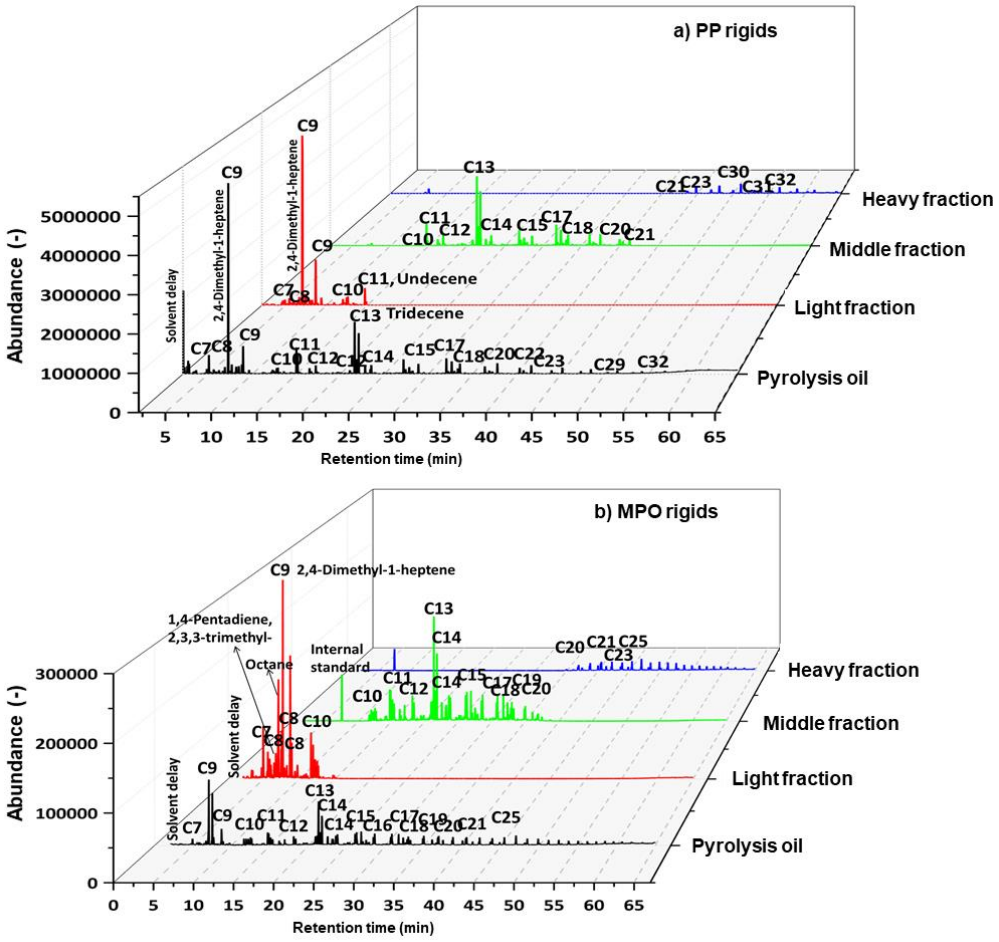

418

419 **Fig. 6**: Comparative GC-MS chromatogram for fractions obtained from a) PP rigids and b) MPO rigids
420 pyrolysis oils.

421 ## 3.5 Chemical functional groups by ATR-FTIR

422 ATR-FTIR spectroscopy was applied to identify functional differences in the organic
423 molecules of pyrolysis oils, light fractions, and middle fractions compared to fossil crude oil,
424 naphtha, and diesel.

425 ### 3.5.1 Pyrolysis and fossil crude oils

426 Fossil crude oil is a complex mixture of hydrocarbons with a broad boiling point trajectory,
427 ranging from gaseous molecules to tar-like materials. Low-concentration impurities can be
428 present, containing oxygen, nitrogen, and sulphur atoms in their structure.

From Fig.7 and Table.4, it can be seen that these oils are typically composed of hydrocarbons containing high amounts of methylene and methyl functional groups. The typical absorption peaks found in the reference sample of crude fossil oil were also observed in all the spectra of the crude pyrolysis oils. However, contrary to fossil crude oil, the investigated pyrolysis oils clearly contain a large amount of unsaturated molecules, indicated by C-H stretching vibrations for sp^2 hybridised carbons observed by a weak peak at 3080 cm^{-1}. Stretching of the C=C bond is indicated by a weak peak around 1644 cm^{-1}. Peaks in the fingerprint region (<1000 cm^{-1}) furthermore give information about the type and degree of substitution of sp^2 hybridised carbons. Peaks for the out-of-plane bending vibrations of C-H are observed at 993 cm^{-1} and 910 cm^{-1} (mono-substituted double bonds), at 967 cm^{-1} (trans disubstituted double bonds), at 888 cm^{-1} (vinylidene) and at 697 cm^{-1} (cis disubstituted double bonds and/or aromatics). Whereas similar peaks were also found in the two pyrolysis oils, but the ratios differ. Relatively low absorbances are noticed for trans-alkenes in all pyrolysis oil samples. Both MPO and PP pyrolysis oils contain a high amount of vinylidenes. These vinylidenes are typically high in PP pyrolysis oil, whereas the mono-substituted alkenes are typical products from PE present in MPO pyrolysis oil (De Amorim et al., 1982;Ylitervo and Richards, 2021). MPO rigids show absorbance at 697 cm^{-1}. GC analysis confirms that this can be assigned aromatics mainly ethylbenzene and styrene, which typically show a strong absorbance at 697cm^{-1}) as in Table. 4. The ratio of peak heights at 1378 cm^{-1} and 1462 cm^{-1} could be seen as an indicator for molecular weight distribution (shorter chains result in more methyl groups relative to methylene groups) or as an indicator for the degree of branching in the sample (more branches implies more methyl groups relative to methylene groups) (Gorce and Spells, 2002;Ferati, 2020). The branching ratio was 0.7, 0.6 and 0.5 for MPO pyrolysis oil, PP pyrolysis oil, and fossil crude oil, respectively. The ATR-FTIR spectrum of crude fossil oil shows an intermediate CH_3/CH_2 ratio, while pyrolysis oils show a somewhat higher CH_3/CH_2 ratio. It is,

however, impossible from the pure ATR-FTIR data to conclude the basic reason for CH_3/CH_2 differences, as this can be due to molecular weight and branching differences.

3.5.2 Light fractions and fossil naphtha

All the light fractions from pyrolysis oil show an increased presence of sp^2 carbons compared to sp^3 carbons, which can be expected since the double bond in a shorter chain will be more pronounced in the ATR-FTIR spectrum. Apart from the sp^2 carbon-hydrogen stretching vibrations at 3080 cm^{-1} originating from aliphatic hydrocarbons, also absorbance is noticed in the MPO light at 3032 $cm^{-1,}$ which is typical for aromatic sp^2 carbon-hydrogen stretching vibrations. This aromaticity is also noticed in the lower ATR-FTIR area, where a strong absorbance is found at 697 cm^{-1} and is confirmed by GC-MS analysis showing high aromatic concentrations in MPO rigids (33.5%, mainly ethylbenzene and styrene). Aromatic compounds are also observed in the fossil naphtha, where weak peaks are present at 796 cm^{-1}, 788 cm^{-1}, 741 cm^{-1}, 728 cm^{-1}, 694 $cm^{-1,}$ and 675 cm^{-1} (these peaks are related to C-H out-of-plane bending vibrations typically found in simple aromatic compounds like toluene, ethylbenzene, and xylenes and are expected to be present in fossil-derived oils (Ito, 2003). All samples show relatively low absorbance for trans-disubstituted alkenes. The PP light mainly shows absorbance for vinylidene double bonds (888 cm^{-1}). MPO rigid shows strong absorbance for vinylidene (888 cm^{-1}) and, to a lesser extent, for mono-substituted alkenes (910 cm^{-1}).

3.5.3 Middle fraction and fossil diesel

The middle fractions from both pyrolysis oils show a less pronounced presence of sp^2 carbons compared to sp^3 carbons, which can be explained by the higher molecular weight distribution compared to light fractions. Both middle fractions show mainly the presence of vinylidenes (888 cm^{-1}) followed by mono-substituted alkenes (910 cm^{-1}). Similar to the conclusion for the light fractions, the presence of double bonds again is the clearest difference between the

pyrolysis oils and fossil oil. Aromatics are present to a lesser extent in the middle fractions than the light fractions.

3.5.4 ATR-FTIR as a method to characterise pyrolysis oils

Similar to GC-MS results, the ATR-FTIR analysis clearly shows that the investigated pyrolysis oils contain a larger number of unsaturated molecules. These unsaturated molecules are both aliphatic and aromatic. The type of sp^2 carbons strongly depends on the type of pyrolysed waste plastic. Pyrolysis of PP gives more vinylidenes, whereas PE pyrolysis gives more mono-substituted alkenes. Contaminations of other nature could give rise to the presence of aromatics (e.g. PS) and acids (e.g. PET). It might be interesting to look in future research for a link between the FTIR data of pyrolysis oils and the composition of the waste plastic used to generate them. It should be stressed however, that this fingerprinting method has some limitations: rather high detection limit (>1%) and overlap with absorptions from contaminants and similar molecules.

491 **Table.4:** Chemical functional groups by FTIR ('x'= present, '±'= small peak present; '-'=not present, *=Assumption) (Silverstein and Bassler, 1962;Socrates, 2004)

Position (cm^{-1})	Assigned bond type	Type of vibration	Crude oil			Light (<175 °C)			Middle (175–360 °C)		
			Fossil oil	MPO rigid	PP rigid	Fossil naphtha 69-175 °C	MPO rigid	PP rigid	Fossil diesel 155-370 °C	MPO rigid	PP rigid
3080	C=**C-H**	stretching	-	x	x	-	x	x	-	x	x
2959	**C-H** (CH_3)	asymmetric stretching	x	x	x	x	x	x	x	x	x
2925	**C-H** (CH_2)	asymmetric stretching	x	x	x	x	x	x	x	x	x
2875	**C-H** (CH_3)	symmetric stretching	x	-	-	x	x	x	x	±	x
2856	**C-H** (CH_2)	symmetric stretching	x	x	x	x			x	x	±
1644	**C=C**	stretching		x	x	-	x	x	-	x	x
1462	**C-H** methylene & methyl	overlap asymmetric in-plane bending CH_2, CH_3 (scissoring)	x	x	x	x	x	x	x	x	x
1378	**C-H** methyl	symmetric in-plane bending (rocking)	x	x	x	x	x	x	x	x	x
993	R_1(**H)C**=C-H_2 (monosubstituted DB)	out-of-plane bending (wagging)	-	x	x	-	x	±	-	x	x
967	**C-H** in $R_1(H)C=C(H)R_2$ (trans disubstituted DB)	out-of-plane bending (wagging)	-	x	x	-	±	±	-	x	x
910	$R_1(H)C=$**C-H$_2$** (monosubstituted DB)	out-of-plane bending (wagging)	-	x	x	-	x	-	-	x	x
888	$R_1(R_2)C=$**C-H$_2$** (vinylidene)	out-of-plane bending (wagging)	-	x	x	-	x	x	-	x	x
811	**Aromatic*	*Out-of-plane bending*	*x*	-	-	-	*x*	-	*x*	-	-
776	$R_1(R_2$ or H)C-**CH_2**-CH_3	symmetric in-plane bending (rocking)	-	±	-	-	x	±	-	±	-
768	**CH_2** for one isolated methylene		x	-	-	x	-	-	x	-	-
742	**CH_2** for two consecutive methylenes		x	-	-	±	±	±	x	x	-
722	**CH_2** for long (>6 C's) linear chains		x	x	x	x	x	-	x	x	-
697	**C-H** in $R_1(H)C=C(H)R_2$ (cis disubstituted) Overlap with aromatic **C-H** (ethylbenzene)	out-of-plane bending (wagging)	±	x	-	±	x	±	x	x	±

492

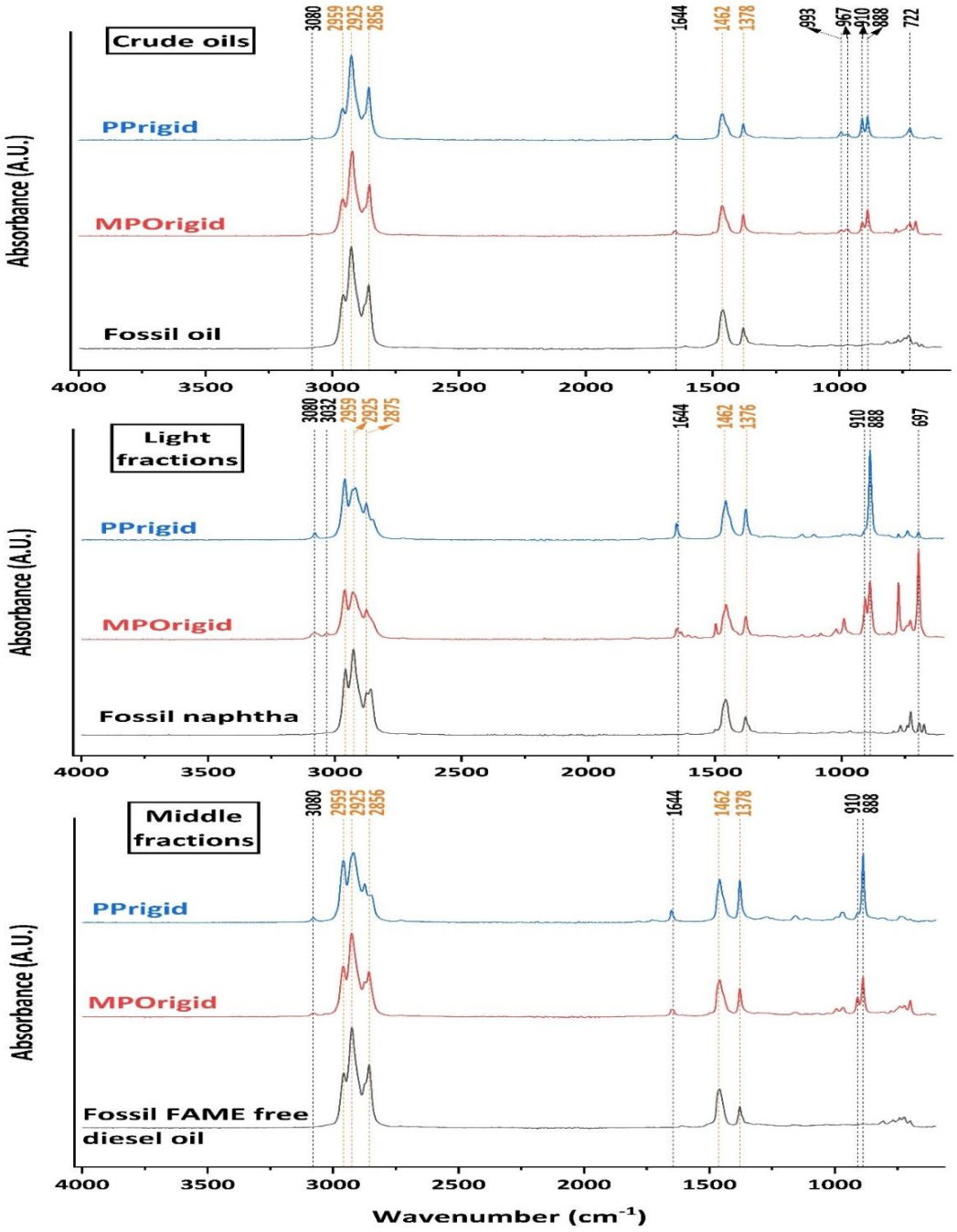

Fig.7: Comparative overview of ATR-FTIR of pyrolysis oils, distilled fractions, and fossil naphtha and diesel.

4. Potential industrial applications of distilled fractions

4.1 Applicability toward steam cracker feedstock

4.1.1 Assessing suitability

To assess the suitability of distilled fractions as steam cracker feedstock, we have summarised hydrocarbon composition (paraffins, olefins, naphthenes & aromatics), heteroatoms, TAN,

halogen, and metal concentrations in the light and middle fractions. The measured values were set out against industrial limits, as highlighted in red in Fig.9 (a, b).

From Fig. 8 (a), it can be seen that the key differences are in the presence of higher quantities of olefins (industrial threshold: <2%), i.e., unsaturation and branching present in all the distilled fractions. Both naphthenes and aromatics contents were lower than the limits/reference sample except for the MPO middle. A large percentage of olefins are undesirable as reactive double bonds in the presence of oxygen and chlorine result in gum formation and corrosion (Gary et al., 2007;George Wypych, 2015). Olefins, naphthenes, and aromatics are major drivers for fouling in steam cracking (Hájeková et al., 2007;Gary et al., 2007;Kopinke et al., 1993b;Kopinke et al., 1993a). Therefore, upgrading technology such as hydrotreatment or blending with fossil-based fractions is required (Zacher et al., 2014;Kusenberg et al., 2022c). The presence of oxygen, nitrogen, and sulphur causes catalyst poisoning. The acceptable limit for N and O in the distilled products is still lower than the detected concentrations. For example, in steam cracking, the limit for N, S, and O is 100 ppm, 50 ppm, and 100 ppm, respectively (Kusenberg et al., 2022b;Gala et al., 2020). Furthermore, TAN values for all the fractions exceed the threshold. Several approaches have been proposed to remove oxygenated acids and nitrogenates. These include solvent extraction and adsorption (Rana et al., 2018;Nasir Shah et al., 2015;Wang et al., 2006). In terms of halogens, chlorine is especially problematic in all distilled fractions, substantially exceeding the threshold limit of 3 ppm for steam crackers. A lower concentration of 3 ppm bromine was detected in the MPO heavy, while fluorine was not detected in any fractions. Chlorine forms highly corrosive acids such as HCl (Kusenberg et al., 2022b). Therefore, dehalogenation of distilled fractions will be especially important prior to the steam cracking.

From Fig 8(b), the most problematic metals for steam crackers are As, Ca, Cu, Fe, Na, Ni, Hg, Pb, Si, and V plotted against industrial limits (Kusenberg et al., 2022d;Kusenberg et al., 2022b).

It can be observed that most of the metals, such as Ca, Cu, Fe, Ni, and V are below industrial limits after distillation in both light and middle fractions except Si, Pb and Na, that are slightly higher than the limits, yet in the case of As and Hg, steam cracker thresholds are below the LOD of the used analytical technique (LOD provided in Table.S2 in the SI). Low Si, Pb, and Na concentrations might still lead to fouling problems in the long run.

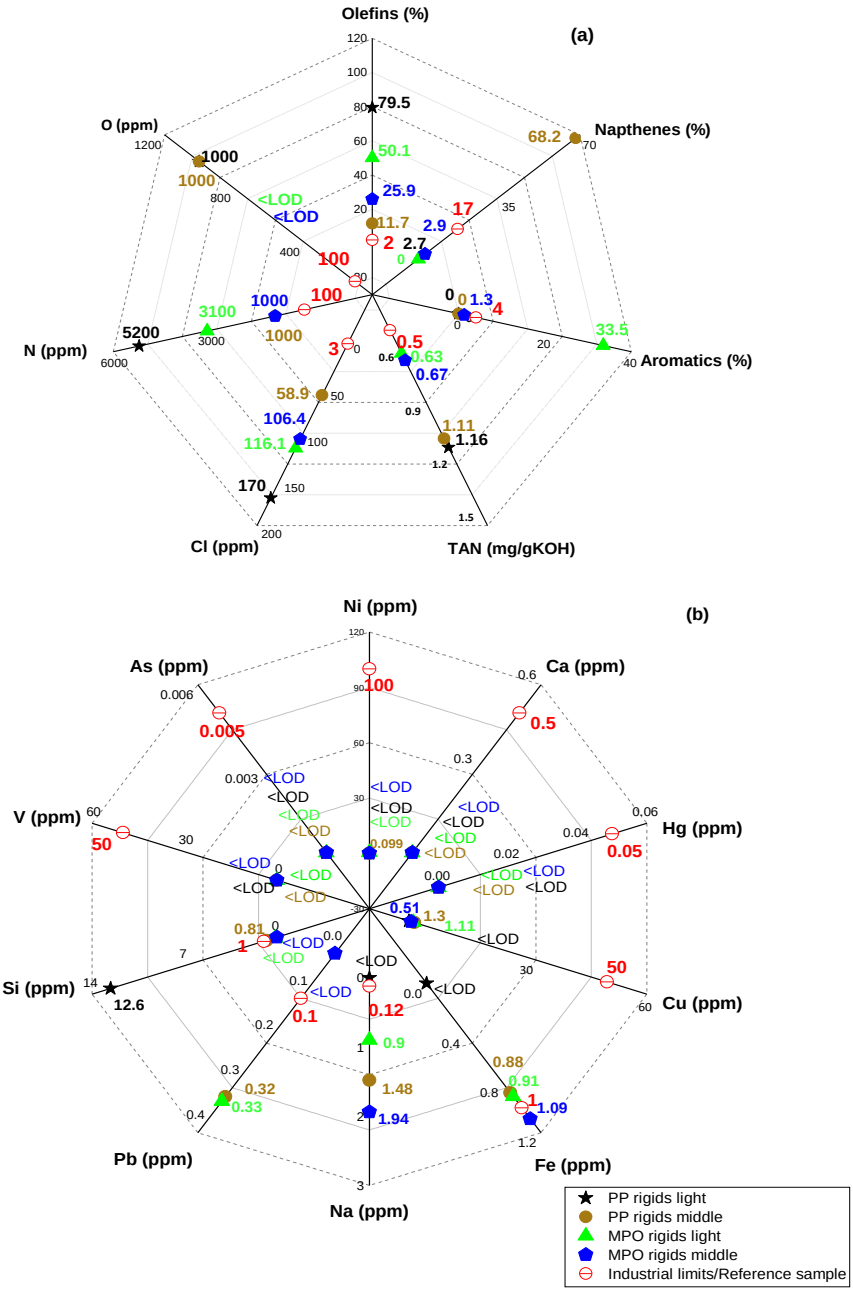

Fig.8: Assessment of light and middle fraction as steam cracker feedstock. The steam cracking threshold values were obtained from our previous studies (Kusenberg et al., 2022d;Kusenberg et al., 2022b).

4.1.2 Steam cracking performance

Fig.9 represents yields of the most important light products (methane, ethylene, propylene, and 1,3-butadiene) obtained from the simulations of distilled fractions used as feedstock for polymer production. It can be observed that the yields of light products from MPO light fraction at both temperature profiles (COT:820 °C, 850 °C) are lower compared to the yields for fossil naphtha. This is due to the presence of high olefins and aromatics content in MPO pyrolysis oil (originated from pyrolysis of non-polyolefins plastic waste i:e PS, PA, EVOH). Product yields of MPO middle fraction are higher in terms of light products. This is caused by the fact that high paraffin, iso-paraffins, and low aromatics and olefins tend to form light olefins in steam cracking. Furthermore, the high yields of middle fractions can be explained by the higher carbon number C_{10}-C_{21} compared to fossil naphtha C_4-C_9 (Kusenberg et al., 2022b;Kusenberg et al., 2022c). Long-chain molecules crack easier hence, a higher conversion is achieved at lower temperatures for middle fractions, also discussed by Hájeková et al. (2007). PP light and middle fractions performed comparably better in terms of ethylene production due to the absence of aromatics in PP pyrolysis oil. Further vital chemicals produced are BTX (benzene, toluene, xylenes), mainly in the case of MPO light and middle fractions. Comprehensive details on the product yields are listed in Table. S5 in the SI.

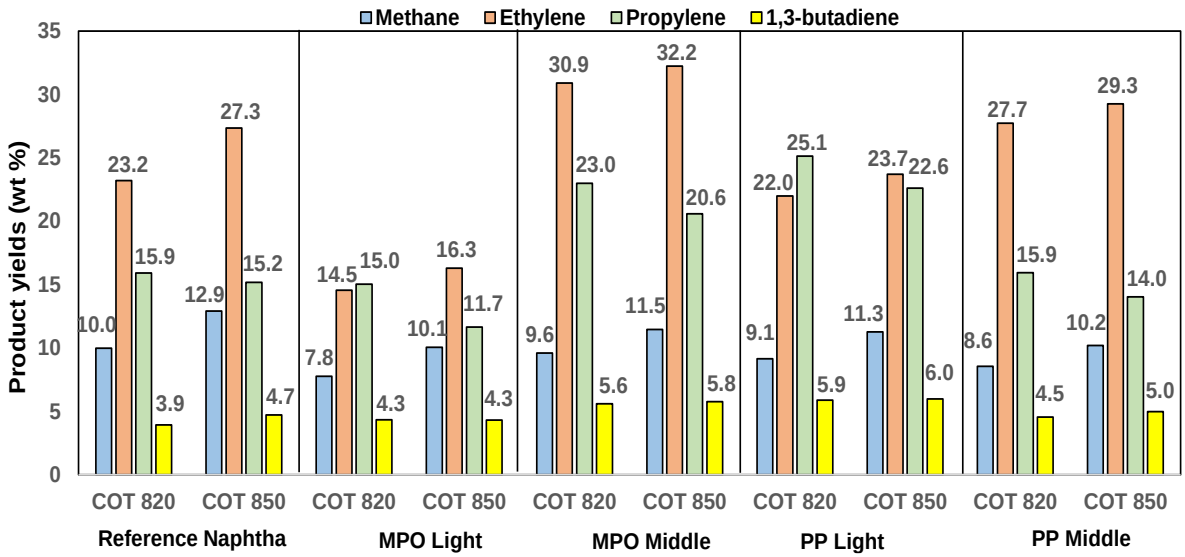

Fig. 9: Simulated steam cracking yields of methane, ethylene, propylene, and 1,3-butadiene from light and middle fractions of PP & MPO pyrolysis oils compared to fossil reference naphtha as a function of the coil temperature (COT: ◦C).

4.2 Applicability as precursors to chemicals

Still, the distillation cuts from crude pyrolysis oils compared to crude oil are significantly different in chemical nature, especially in the case of PP-containing waste, so it is worth discussing which is the best application. From the ATR-FTIR spectra, it is clear that double bonds (alkenes) in both PP and MPO pyrolysis oil are abundantly present, and distillation increases the concentration of olefins in light and middle fractions by separating heavy fractions (≥C21). These olefins are reactive and thus interesting for synthesising various commercial products, such as solvents, polymers, monomers, surfactants, and detergents (Upare et al., 2017). Important precursors are linear alfa olefins (LAO; terminal double bonds). Except for MPO light, all the fractions have more than 10% LAOs. Other precursors are internal olefins, cyclic olefins, and vinylidenes abundantly present in both PP and MPO light fractions, as in Table.S4 in the SI. (Goris et al., 2022;Zhao et al., 2020). Depending on the applications, the chain length of the functionalised molecules could be short or long. Commercial reactions of olefins typically include addition, alkylation, oxidation, oxo reactions (hydroformylations), and halogenation (Bruice, 2014). We discuss some of the commercial applications of olefins that might be explorable based on polyolefin (MPO/PP) pyrolysis oil composition.

From Fig.10, considering the light fractions, (1) LAOs C_4-C_8 are precursors to fatty acids such as lactic acid, ketones and aldehydes (Franke et al., 2012). (2) Epoxidation of lower C_4-C_9 olefins produces intermediates and antifreeze agents, such as glycols (Aida et al., 2022;Alvear et al., 2021). (3) C_5-C_{10} LAOs and internal olefins can be functionalised via hydroformylation with syn-gas and rhodium catalysts to produce aldehydes and oxo-alcohols. These functionalities can be transformed into plasticisers, surfactants, solvents, and acrylates (Zhao

et al., 2020). Furthermore, C_{10} aldehydes find their application in making perfumery chemicals (Franke et al., 2012). (4,5) C_{10}-C_{16} olefins in the middle fractions of waste plastic pyrolysis oils are valuable precursors for producing detergent alcohols due to their high conversions (>86%), as discussed in the recent patent by Goris et al. (2022). Main commercial products are laundry and dishwashing cleaners, surfactants and plasticisers. (6) Both linear and internal C_{16}-C_{24} olefins produce paraffines that are used as precursors to produce oil field chemicals, solvents and additives (Oxo Chemicals, 2021;Sharma and Jasra, 2015;ExxonMobil, 2023;Zhao et al., 2020). The heavy fraction (>C_{21}) can be valorised as wax in candles making and PVC pipes formulation)(Euroceras, 2023;Bekker et al., 2022).

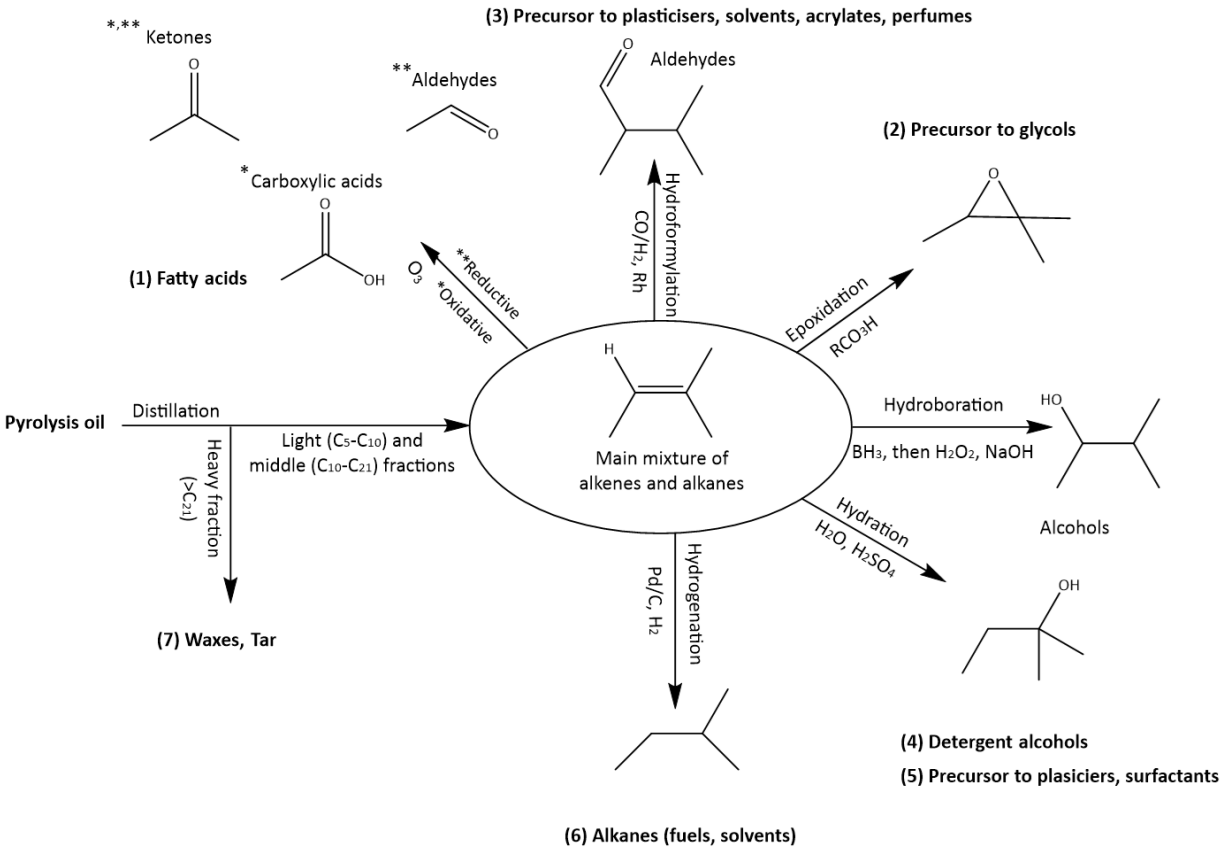

Fig.10: Mapping chemical reactions for producing precursors to chemicals from light and middle fractions of PP & MPO pyrolysis oils. The reaction map is produced from the chemistry of alkenes (Bruice, 2014;James, 2023).

Further research should investigate the integration of pyrolysis oil in existing refineries and petrochemical infrastructure to minimise additional processing and separation costs. Carbon footprint analysis of the process is necessary for sustainability and to help the government to decide on tax reductions and the provision of green premiums. Market assessment of chemicals should be studied since the energy transition will reduce demand for oil products as fuel but increase opportunities to capture the growing demand for chemicals (Huysveld et al., 2022;Civancik-Uslu et al., 2021;Larrain et al., 2020).

5. Conclusion and outlook

Vacuum fractional distillation of two types of post-consumer plastic-derived pyrolysis oil resulted in narrow carbon distribution and purified fractions. The chemical composition of the light fractions derived from PP and MPO pyrolysis oil showed high amounts of olefins (>48%) compared to petroleum naphtha, while aromatics and naphthenes were mainly present in MPO fractions and PP middle fraction, respectively. Consequently, hydrotreatment would be the next necessary upgradation step for steam cracking. On the other hand, olefins are interesting molecules to functionalise for their applications as precursors to produce commercial chemicals. Fractional distillation allows the removal of most of the undesirable metal contaminations (>97.5%), indicating significant purification. This shows that these fractions will perform better in terms of coke formation, catalyst poisoning, and fouling compared to pyrolysis oil. The elevated oxygen, nitrogen (>100 ppm), TAN number (>0.5 mgKOH/g), and chlorine contents (>10 ppm) indicate that oxygenates, nitrogenates, and total chlorides exceed the limits. Therefore, steam cracking and chemical conversion require further clean-up techniques such as adsorption or extraction to minimise operational problems. The simulated steam cracking yields of distilled fractions were comparable to reference fossil naphtha, showing that post-consumer pyrolysis is viable feedstock.

Acknowledgements

The research leading to these results is funded by the Catalisti-ICON project, "Plastics to Precious Chemicals (P2PC)", Project code: HBC.2019.0003 funded by Flanders Innovation & Entrepreneurship (VLAIO), the European Research Council under the European Unions Horizon-2020 research and innovation program/ERC Grant Agreements No. 818607 "ERC OPTIMA" and Higher Education Commission of Pakistan (HEC) for scholarship under "HRDI-UESTPS/UETS" program.

Declaration of competing interest

The authors declare no conflict of interest.

CRediT authorship contribution statement

Waheed Zeb: conceptualisation, methodology, analysis, investigation, writing – original draft, review & editing. **Martijn Roosen:** methodology, investigation, writing–review & editing. **Pieter Knockaert**: design & installation of distillation setup. **Daniël Withoeck:** steam cracking simulations, writing– review & editing. **Marvin Kusenberg:** resources, writing– review & editing. **Sven Janssens:** analysis, writing– review & editing. **Joël Hogie:** supervision, writing– review & editing. **Pieter Billen**: project administration, review and editing. **Serge Tavernier**: project administration, review & editing. **Kevin M. Van Geem:** project administration, writing – review & editing. **Steven De Meester:** Conceptualisation, funding acquisition, project administration, supervision, writing – review & editing.

References

AIDA, K., HIRAO, M., FUNABASHI, A., SUGIMURA, N., OTA, E. & YAMAGUCHI, J. 2022. Catalytic reductive ring opening of epoxides enabled by zirconocene and photoredox catalysis. *Chem,* 8**,** 1762-1774.

AL-SALEM, S., LETTIERI, P. & BAEYENS, J. 2010. The valorization of plastic solid waste (PSW) by primary to quaternary routes: From re-use to energy and chemicals. *Progress in Energy and Combustion Science,* 36**,** 103-129.

ALI, M. F. & ABBAS, S. 2006. A review of methods for the demetallization of residual fuel oils. *Fuel Processing Technology,* 87**,** 573-584.

ALVEAR, M., FORTUNATO, M. E., RUSSO, V., ERANEN, K., DI SERIO, M., LEHTONEN, J., RAUTIAINEN, S., MURZIN, D. & SALMI, T. 2021. Continuous liquid-phase epoxidation of ethylene with hydrogen peroxide on a titanium-silicate catalyst. *Industrial & Engineering Chemistry Research,* 60**,** 9429-9436.

ALVISI, P. P. & LINS, V. F. 2011. An overview of naphthenic acid corrosion in a vacuum distillation plant. *Engineering Failure Analysis,* 18**,** 1403-1406.

ASTM D2892 2019. Standard test method for distillation of crude petroleum (15-theoretical plate column). *Annual Book of Standards.*

BALLICE, L. & REIMERT, R. 2002. Classification of volatile products from the temperature-programmed pyrolysis of polypropylene (PP), atactic-polypropylene (APP) and thermogravimetrically derived kinetics of pyrolysis. *Chemical Engineering and Processing: Process Intensification,* 41**,** 289-296.

BEKKER, M., ROBERTSON, D., DUVESKOG, H. & VAN REENEN, A. J. 2022. Performance Mapping toward Optimal Addition Levels and Processing Conditions for Different Types of Hydrocarbon Waxes Typically Used as External Lubricants in Sn-Stabilized PVC Pipe Formulations. *ACS omega,* 7**,** 22199-22209.

BRUICE, P. Y. 2014. Organic chemistry, 7th International Edition. Prentice Hall.

CHANDRASEKARAN, S. R. & SHARMA, B. K. 2019. From waste to resources: How to integrate recycling into the production cycle of plastics. *Plastics to Energy.* Elsevier.

CHEN, Y., AWASTHI, A. K., WEI, F., TAN, Q. & LI, J. 2021. Single-use plastics: Production, usage, disposal, and adverse impacts. *Sci Total Environ,* 752**,** 141772.

CIVANCIK-USLU, D., NHU, T. T., VAN GORP, B., KRESOVIC, U., LARRAIN, M., BILLEN, P., RAGAERT, K., DE MEESTER, S., DEWULF, J. & HUYSVELD, S. 2021. Moving from linear to circular household plastic packaging in Belgium: Prospective life cycle assessment of mechanical and thermochemical recycling. *Resources, Conservation and Recycling,* 171**,** 105633.

CZAJCZYŃSKA, D., ANGUILANO, L., GHAZAL, H., KRZYŻYŃSKA, R., REYNOLDS, A., SPENCER, N. & JOUHARA, H. 2017. Potential of pyrolysis processes in the waste management sector. *Thermal science and engineering progress,* 3**,** 171-197.

DAO THI, H., DJOKIC, M. R. & VAN GEEM, K. M. 2021. Detailed Group-Type Characterization of Plastic-Waste Pyrolysis Oils: By Comprehensive Two-Dimensional Gas Chromatography Including Linear, Branched, and Di-Olefins. *Separations,* 8**,** 103.

DE AMORIM, M. S. P., COMEL, C. & VERMANDE, P. 1982. Pyrolysis of polypropylene: I. Identification of compounds and degradation reactions. *Journal of Analytical and Applied Pyrolysis,* 4**,** 73-81.

DIAZ-SILVARREY, L. S., MCMAHON, A. & PHAN, A. N. 2018. Benzoic acid recovery via waste poly (ethylene terephthalate)(PET) catalytic pyrolysis using sulphated zirconia catalyst. *Journal of analytical and applied pyrolysis,* 134**,** 621-631.

DIJKMANS, T., DJOKIC, M. R., VAN GEEM, K. M. & MARIN, G. B. 2015. Comprehensive compositional analysis of sulfur and nitrogen containing compounds in shale oil using GC× GC–FID/SCD/NCD/TOF-MS. *Fuel,* 140**,** 398-406.

DJOKIC, M. R., DIJKMANS, T., YILDIZ, G., PRINS, W. & VAN GEEM, K. M. 2012. Quantitative analysis of crude and stabilized bio-oils by comprehensive two-dimensional gas-chromatography. *J Chromatogr A,* 1257**,** 131-40.

DOGU, O., PELUCCHI, M., VAN DE VIJVER, R., VAN STEENBERGE, P. H., D'HOOGE, D. R., CUOCI, A., MEHL, M., FRASSOLDATI, A., FARAVELLI, T. & VAN GEEM, K. M. 2021. The chemistry of chemical recycling of solid plastic waste via pyrolysis and gasification: State-of-the-art, challenges, and future directions. *Progress in Energy and Combustion Science,* 84**,** 100901.

EBNESAJJAD, S. 2020. *Chapter-8,Fluorinated Additives,*

Introduction to fluoropolymers: materials, technology, and applications, William Andrew.

EUROCERAS. 2023. *Polyolefin waxes* [Online]. Available: https://euroceras.com/products/ceralener-polyolefins-waxes/ [Accessed 25/03/2023].

EUROPEAN COMMITTEE 2013. Automotive Fuels–Diesel–Requirements and Test Methods. *SS-EN*.

EXXONMOBIL. 2023. *Linear Alpha Olefin* [Online]. Available: https://www.exxonmobilchemical.com/en/resources/library/library-detail/91695/elevexx_factsheet [Accessed 23/03/2023].

FAUSSONE, G. C. 2018. Transportation fuel from plastic: Two cases of study. *Waste Manag,* 73**,** 416-423.

FAUSSONE, G. C. & CECCHI, T. 2022. Chemical recycling of plastic marine litter: first analytical characterization of the pyrolysis oil and of its fractions and comparison with a commercial marine gasoil. *Sustainability,* 14**,** 1235.

FERATI, F. 2020. Structural information from ratio bands in the FTIR spectra of long chain and branched alkanes in petroleum samples. *Journal of Enveronmental Treatment Techniques,* 8**,** 1140-1143.

FRANKE, R., SELENT, D. & BORNER, A. 2012. Applied hydroformylation. *Chem Rev,* 112**,** 5675-732.

GALA, A., GUERRERO, M., GUIRAO, B., DOMINE, M. E. & SERRA, J. M. 2020. Characterization and Distillation of Pyrolysis Liquids Coming from Polyolefins Segregated of MSW for Their Use as Automotive Diesel Fuel. *Energy & Fuels,* 34**,** 5969-5982.

GARY, J. H., HANDWERK, J. H., KAISER, M. J. & GEDDES, D. 2007. *Petroleum refining: technology and economics*, CRC press.

GEORGE WYPYCH 2015. *4 - PRINCIPLES OF THERMAL DEGRADATION, PVC Degradation and Stabilization* ChemTec Publishing.

GEYER, R., JAMBECK, J. R. & LAW, K. L. 2017. Production, use, and fate of all plastics ever made. *Science advances,* 3**,** e1700782.

GORCE, J.-P. & SPELLS, S. J. 2002. Structural information from progression bands in the FTIR spectra of long chain n-alkanes. *Polymer,* 43**,** 4043-4046.

GORIS, H. K. T., LI, C., BIEN, D., CARPENTER, A. E. & DIAZ, C. M. 2022. *METHODSFOR PRODUCING HIGHER ALCOHOLS FROM WASTE PLASTIC PYROLYSIS OIL AND THE HIGHER ALCOHOLS OBTAINED THEREFROM*. EP2021078784W.

GRAMS, J. 2020. Chromatographic analysis of bio-oil formed in fast pyrolysis of lignocellulosic biomass. *Reviews in Analytical Chemistry,* 39**,** 65-77.

HÁJEKOVÁ, E., MLYNKOVÁ, B., BAJUS, M. & ŠPODOVÁ, L. 2007. Copyrolysis of naphtha with polyalkene cracking products; the influence of polyalkene mixtures composition on product distribution. *Journal of analytical and applied pyrolysis,* 79**,** 196-204.

HORODYTSKA, O., VALDES, F. J. & FULLANA, A. 2018. Plastic flexible films waste management - A state of art review. *Waste Manag,* 77**,** 413-425.

HUYSVELD, S., RAGAERT, K., DEMETS, R., NHU, T. T., CIVANCIK-USLU, D., KUSENBERG, M., VAN GEEM, K., DE MEESTER, S. & DEWULF, J. 2022. Technical and market substitutability of recycled materials: Calculating the environmental benefits of mechanical and chemical recycling of plastic packaging waste. *Waste Management,* 152**,** 69-79.

ITO, S. 2003. Analysis of aromatic hydrocarbons in gasoline and naphtha with the Agilent 6820 series gas chromatograph and a single polar capillary column. *Agilent Technologies.*

JAHIRUL, M., FAISAL, F., RASUL, M., SCHALLER, D., KHAN, M. & DEXTER, R. 2022. Automobile fuels (diesel and petrol) from plastic pyrolysis oil—Production and characterisation. *Energy Reports,* 8**,** 730-735.

JAMES, A. 2023. *A Map of Addition and Oxidative Cleavage Reactions of Alkenes* [Online]. Available: https://www.masterorganicchemistry.com/2014/01/21/synthesis-reactions-of-alkenes/ [Accessed 28/3/2023].

JAMRADLOEDLUK, J. & LERTSATITTHANAKORN, C. 2014. Characterization and utilization of char derived from fast pyrolysis of plastic wastes. *Procedia Engineering,* 69**,** 1437-1442.

KARONIS, D., LOIS, E., STOURNAS, S. & ZANNIKOS, F. 1998. Correlations of exhaust emissions from a diesel engine with diesel fuel properties. *Energy & Fuels,* 12**,** 230-238.

KNOTHE, G. & STEIDLEY, K. R. 2005. Kinematic viscosity of biodiesel fuel components and related compounds. Influence of compound structure and comparison to petrodiesel fuel components. *Fuel,* 84**,** 1059-1065.

KOPINKE, F. D., ZIMMERMANN, G., REYNIERS, G. C. & FROMENT, G. F. 1993a. *Industrial & Engineering Chemistry Research,* 32**,** 56-61.

KOPINKE, F. D., ZIMMERMANN, G., REYNIERS, G. C. & FROMENT, G. F. 1993b. Relative rates of coke formation from hydrocarbons in steam cracking of naphtha. 3. Aromatic hydrocarbons. *Industrial & Engineering Chemistry Research,* 32**,** 2620-2625.

KUSCH, P. 2017. Application of pyrolysis-gas chromatography/mass spectrometry (Py-GC/MS).

KUSENBERG, M., ESCHENBACHER, A., DJOKIC, M. R., ZAYOUD, A., RAGAERT, K., DE MEESTER, S. & VAN GEEM, K. M. 2022a. Opportunities and challenges for the application of post-consumer plastic waste pyrolysis oils as steam cracker feedstocks: To decontaminate or not to decontaminate? *Waste Management,* 138**,** 83-115.

KUSENBERG, M., FAUSSONE, G. C., THI, H. D., ROOSEN, M., GRILC, M., ESCHENBACHER, A., DE MEESTER, S. & VAN GEEM, K. M. 2022b. Maximizing olefin production via steam cracking of distilled pyrolysis oils from difficult-to-recycle municipal plastic waste and marine litter. *Sci Total Environ,* 838**,** 156092.

KUSENBERG, M., ROOSEN, M., ZAYOUD, A., DJOKIC, M. R., DAO THI, H., DE MEESTER, S., RAGAERT, K., KRESOVIC, U. & VAN GEEM, K. M. 2022c. Assessing the feasibility of chemical recycling via steam cracking of untreated plastic waste pyrolysis oils: Feedstock impurities, product yields and coke formation. *Waste Manag,* 141**,** 104-114.

KUSENBERG, M., ZAYOUD, A., ROOSEN, M., THI, H. D., ABBAS-ABADI, M. S., ESCHENBACHER, A., KRESOVIC, U., DE MEESTER, S. & VAN GEEM, K. M. 2022d. A comprehensive experimental investigation of plastic waste pyrolysis oil quality and its dependence on the plastic waste composition. *Fuel Processing Technology,* 227**,** 107090.

LARRAIN, M., VAN PASSEL, S., THOMASSEN, G., KRESOVIC, U., ALDERWEIRELDT, N., MOERMAN, E. & BILLEN, P. 2020. Economic performance of pyrolysis of mixed

plastic waste: Open-loop versus closed-loop recycling. *Journal of Cleaner Production,* 270**,** 122442.
LEE, D., NAM, H., WANG, S., KIM, H., KIM, J. H., WON, Y., HWANG, B. W., KIM, Y. D., NAM, H., LEE, K. H. & RYU, H. J. 2021. Characteristics of fractionated drop-in liquid fuel of plastic wastes from a commercial pyrolysis plant. *Waste Manag,* 126**,** 411-422.
LOPEZ, G., ARTETXE, M., AMUTIO, M., BILBAO, J. & OLAZAR, M. 2017. Thermochemical routes for the valorization of waste polyolefinic plastics to produce fuels and chemicals. A review. *Renewable and Sustainable Energy Reviews,* 73**,** 346-368.
MAJANO, G., NG, E.-P., LAKISS, L. & MINTOVA, S. 2011. Nanosized molecular sieves utilized as an environmentally friendly alternative to antioxidants for lubricant oils. *Green Chemistry,* 13**,** 2435-2440.
MANGESH, V., PADMANABHAN, S., TAMIZHDURAI, P. & RAMESH, A. 2020. Experimental investigation to identify the type of waste plastic pyrolysis oil suitable for conversion to diesel engine fuel. *Journal of Cleaner Production,* 246**,** 119066.
MEYS, R., FRICK, F., WESTHUES, S., STERNBERG, A., KLANKERMAYER, J. & BARDOW, A. 2020. Towards a circular economy for plastic packaging wastes–the environmental potential of chemical recycling. *Resources, Conservation and Recycling,* 162**,** 105010.
MURPHY, F., MCDONNELL, K., BUTLER, E. & DEVLIN, G. 2012. The evaluation of viscosity and density of blends of Cyn-diesel pyrolysis fuel with conventional diesel fuel in relation to compliance with fuel specifications EN 590: 2009. *Fuel,* 91**,** 112-118.
NASIR SHAH, S., MUTALIB, M. I. A., PILUS, R. B. M. & LETHESH, K. C. 2015. Extraction of naphthenic acid from highly acidic oil using hydroxide-based ionic liquids. *Energy & Fuels,* 29**,** 106-111.
OXO CHEMICALS. 2021. *Chemical Economics Handbook* [Online]. Available: https://www.spglobal.com/commodityinsights/en/ci/products/oxo-chemical-economics-handbook.html [Accessed 13/03/2023].
PARK, K.-B., JEONG, Y.-S., GUZELCIFTCI, B. & KIM, J.-S. 2020. Two-stage pyrolysis of polystyrene: Pyrolysis oil as a source of fuels or benzene, toluene, ethylbenzene, and xylenes. *Applied Energy,* 259**,** 114240.
PLASTIC ENERGY. 2021. *Plastic Energy Spain* [Online]. Available: https://plasticenergy.com/technology/#patented-technology [Accessed 10/10/2021 2021,].
PLASTIC EUROPE 2022. An analysis of European plastics production, demand and waste data, Plastics – the Facts 2022.
PLEHIERS, P. P., SYMOENS, S. H., AMGHIZAR, I., MARIN, G. B., STEVENS, C. V. & VAN GEEM, K. M. 2019. Artificial intelligence in steam cracking modeling: a deep learning algorithm for detailed effluent prediction. *Engineering,* 5**,** 1027-1040.
RAGAERT, K., DELVA, L. & VAN GEEM, K. 2017. Mechanical and chemical recycling of solid plastic waste. *Waste Manag,* 69**,** 24-58.
RANA, B. S., CHO, D.-W., CHO, K. & KIM, J.-N. 2018. Total Acid Number (TAN) reduction of high acidic crude oil by catalytic esterification of naphthenic acids in fixed-bed continuous flow reactor. *Fuel,* 231**,** 271-280.
RANNAVESKI, R., JÄRVIK, O. & OJA, V. 2016. A new method for determining average boiling points of oils using a thermogravimetric analyzer. *Journal of Thermal Analysis and Calorimetry,* 126**,** 1679-1688.

REOIL. 2021. *ReOil® pilot plant OMV Austria* [Online]. Available: https://www.omv.com/en/blog/reoil-getting-crude-oil-back-out-of-plastic [Accessed 10/10/2021].
RIGIDS PLASTIC. 2023. *Chapter 1: Collection* [Online]. American Legal Publisher. Available: https://codelibrary.amlegal.com/codes/newyorkcity/latest/NYCrules/0-0-0-132489 [Accessed 25/02/2023].
ROOSEN, M., MYS, N., KUSENBERG, M., BILLEN, P., DUMOULIN, A., DEWULF, J., VAN GEEM, K. M., RAGAERT, K. & DE MEESTER, S. 2020. Detailed Analysis of the Composition of Selected Plastic Packaging Waste Products and Its Implications for Mechanical and Thermochemical Recycling. *Environ Sci Technol,* 54**,** 13282-13293.
SEO, Y.-H. & SHIN, D.-H. 2002. Determination of paraffin and aromatic hydrocarbon type chemicals in liquid distillates produced from the pyrolysis process of waste plastics by isotope-dilution mass spectrometry. *Fuel,* 81**,** 2103-2112.
SHARMA, S. K. & JASRA, R. V. 2015. Aqueous phase catalytic hydroformylation reactions of alkenes. *Catalysis Today,* 247**,** 70-81.
SHARUDDIN, S. D. A., ABNISA, F., DAUD, W. M. A. W. & AROUA, M. K. 2016. A review on pyrolysis of plastic wastes. *Energy conversion and management,* 115**,** 308-326.
SHER, E. 1998. *Handbook of air pollution from internal combustion engines: pollutant formation and control*, Academic Press.
SILVERSTEIN, R. M. & BASSLER, G. C. 1962. Spectrometric identification of organic compounds. *Journal of Chemical Education,* 39**,** 546.
SOCRATES, G. 2004. *Infrared and Raman characteristic group frequencies: tables and charts*, John Wiley & Sons.
SPEIGHT, J. G. 2019. *Chapter 3 - Hydrocarbons from crude oil, Handbook of industrial hydrocarbon processes*, Gulf Professional Publishing.
SYMOENS, S. H., OLAHOVA, N., MUÑOZ GANDARILLAS, A. S. E., KARIMI, H., DJOKIC, M. R., REYNIERS, M.-F. O., MARIN, G. B. & VAN GEEM, K. M. 2018. State-of-the-art of coke formation during steam cracking: Anti-coking surface technologies. *Industrial & Engineering Chemistry Research,* 57**,** 16117-16136.
THAHIR, R., ALTWAY, A. & JULIASTUTI, S. R. 2019. Production of liquid fuel from plastic waste using integrated pyrolysis method with refinery distillation bubble cap plate column. *Energy Reports,* 5**,** 70-77.
UGDULER, S., VAN GEEM, K. M., ROOSEN, M., DELBEKE, E. I. P. & DE MEESTER, S. 2020. Challenges and opportunities of solvent-based additive extraction methods for plastic recycling. *Waste Manag,* 104**,** 148-182.
VAN GEEM, K. M., PYL, S. P., REYNIERS, M. F., VERCAMMEN, J., BEENS, J. & MARIN, G. B. 2010. On-line analysis of complex hydrocarbon mixtures using comprehensive two-dimensional gas chromatography. *J Chromatogr A,* 1217**,** 6623-33.
WANG, Y., CHU, Z., QIU, B., LIU, C. & ZHANG, Y. 2006. Removal of naphthenic acids from a vacuum fraction oil with an ammonia solution of ethylene glycol. *Fuel,* 85**,** 2489-2493.
YAN, D., WANG, W.-J. & ZHU, S. 1999. Effect of long chain branching on rheological properties of metallocene polyethylene. *Polymer,* 40**,** 1737-1744.
YANG, R., CHRISTENSEN, P., EGERTON, T. & WHITE, J. 2010. Degradation products formed during UV exposure of polyethylene–ZnO nano-composites. *Polymer Degradation and Stability,* 95**,** 1533-1541.
YLITERVO, P. & RICHARDS, T. 2021. Gaseous products from primary reactions of fast plastic pyrolysis. *Journal of Analytical and Applied Pyrolysis,* 158**,** 105248.

ZACHER, A. H., OLARTE, M. V., SANTOSA, D. M., ELLIOTT, D. C. & JONES, S. B. 2014. A review and perspective of recent bio-oil hydrotreating research. *Green Chemistry,* 16**,** 491-515.

ZAYOUD, A., DAO THI, H., KUSENBERG, M., ESCHENBACHER, A., KRESOVIC, U., ALDERWEIRELDT, N., DJOKIC, M. & VAN GEEM, K. M. 2022. Pyrolysis of end-of-life polystyrene in a pilot-scale reactor: Maximizing styrene production. *Waste Manag,* 139**,** 85-95.

ZHANG, A., MA, Q., WANG, K., LIU, X., SHULER, P. & TANG, Y. 2006. Naphthenic acid removal from crude oil through catalytic decarboxylation on magnesium oxide. *Applied Catalysis A: General,* 303**,** 103-109.

ZHAO, D., WANG, X., MILLER, J. B. & HUBER, G. W. 2020. The Chemistry and Kinetics of Polyethylene Pyrolysis: A Process to Produce Fuels and Chemicals. *ChemSusChem,* 13**,** 1764-1774.